National Defence
Research and
Development Branch

Défense nationale
Bureau de recherche
et développement

TECHNICAL MEMORANDUM 89/222
September 1989

AD-A214 764

A REVIEW OF THE THEORY AND METHODS FOR DETERMINING DYNAMIC PULSE BUCKLING OF CYLINDRICAL SHELLS

NEIL G. PEGG

DTIC
ELECTE
NOV 2 9 1989
S E D

**Defence
Research
Establishment
Atlantic**

**Centre de
Recherches pour la
Défense
Atlantique**

Canadä

DEFENCE RESEARCH ESTABLISHMENT ATLANTIC

CENTRE DE RECHERCHES POUR LA DÉFENSE ATLANTIQUE

National Defence
Research and
Development Branch

Défense nationale
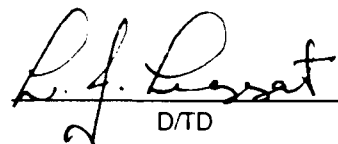Bureau de recherche
et développement

A REVIEW OF THE THEORY AND METHODS
FOR DETERMINING DYNAMIC
PULSE BUCKLING OF CYLINDRICAL SHELLS

Neil G. Pegg

September 1989

Approved by L.J. Leggat
Director/Technical Division

Distribution Approved by

D/TD

TECHNICAL MEMORANDUM 89/222

Defence
Research
Establishment
Atlantic

Centre de
Recherches pour la
Défense
Atlantique

Canada

Abstract

A review of theoretical developments in predicting the buckling response of cylinders subject to impulsive loads is presented. Most of this theory deals with axisymmetric, radial impulses on cylinders. The development of solutions for the critical modes and loading magnitudes which produce excessive growth of displacements are reviewed. Existing theories cover the specific cases of either entirely elastic or entirely plastic material behaviour for infinite length and short cylindrical shells. The resultant theories are applied to various shell geometries to investigate influencial parameters. A review of numerical finite element and finite difference studies which investigate dynamic pulse buckling is also given. The requirements to examine dynamic buckling of more complex structures such as ring stiffened cylinders are discussed.

Résumé

Un examen des perfectionnements théoriques pour la prédiction de la réaction au flambage des cylindres soumis à des impulsions de charge est présenté. La plus grande partie de cette théorie a porté sur les impulsions radiales, axisymétriques exercées sur les cylindres. On y examine aussi les solutions mises au point pour les amplitudes de charges et les modes critiques qui produisent des déplacements sans limites. Les théories existantes portent sur des cas précis de comportement des matériaux entièrement élastiques ou entièrement plastiques pour des enveloppes cylindriques courtes et des longueur infinie. Les théories qui en découlent sont appliquées à différentes géométries d'enveloppes afin d'étudier les paramètres d'influence. Un examen des étude d'éléments finis numériques et d'écarts finis relatives à l'étude du flambage par impulsion dynamique est aussi présenté. On y traite des exigences pour l'étude du flambage dynamique de structures plus complexes comme des cylindres renforcés de frettes.

Contents

List of Figures

Notation

a	shell radius to mid thickness
$a_n(\tau), b_n(\tau)$	asymmetric amplitudes of motion
a_0, w_0	radial hoop mode amplitude
$A_{n_{cr}}$	displacement amplification from autoparametric excitation of flexural mode
$A_n(\zeta), B_n(\zeta)$	amplification functions for displacement and velocity imperfections
B_n	$= v_0 \alpha_n / p_n$
c	speed of sound in material $= \sqrt{\frac{E_l}{\rho}}$, constant in equation (159)
c_h	$= \sqrt{E_h / \rho}$
$C(q), f, q, q_0, c, \bar{n}$	coefficients defined in equation (161)
$C_1, C_2, C_3, C_4, C_5, C_6$	constants defined in reference 17
$d\lambda$	differential arc length of shell
D_n	$= v_0 \beta_n / p_n$
D	$\frac{12E}{(1-\nu^2)}$
E_h	strain hardening tangent modulus
E_l	equivalent Young's Modulus $= \frac{E}{1-\nu^2}$
E	Young's Modulus
E_t	tangent modulus
f_n, g_n	generalized variables, dependent on n
F	stress function
h	shell thickness
h_o	shell thickness
I	moment of inertia

I_A	asymptotic peak impulse
I_{fi}	critical impulse from Dirac delta function
I_c	peak impulse amplitude
k	variable length parameter
K_1	$= 2(1 - k + k^2)$
K_2	$(3K_1/2)^{1/2}$
K_3	$(2 - k)/K_1$
K	material curve parameter defined as $\frac{\sigma}{E_t}$
L	length of shell
l	nondimensional length $= L/a$
M_i	resultant moment in i direction
m	mass of shell material$= \rho h$
n	circumferential harmonic wave number
n_{cr}	circumferential harmonic of greatest unbounded growth
N_i	resultant membrane force in i coordinate direction
p_n^2	$= (n^2 - 1)(n^2 - s^2)$
p	stability parameter $= V_0/c\alpha$
P	radial pressure
$P_0(\tau)$	axisymmetric pressure amplitude
$P_n(\tau)$	asymmetric pressure amplitude
P_A	asymptotic peak pressure
p_0	minimum pulse amplitude to cause buckling
P_n	$= \frac{4\alpha^2 \gamma V_0 K_2 n^4}{3(2-k)a}$
p, D	constants defining material curves that are strain rate dependent

Q	shear force
Q_n	parameter of Bessel equation, defined in text
r	deformed shell radius $= a - w_o$
R_n^2	parameter of Bessel equation, defined in text
R	radius of deformed motion, $= a(1 - w)$
S	circumferential membrane force
s^2	nondimensional shell parameter$= Sa^2/E_h I = 12\sigma a^2/E_h h^2$ for plastic flow buckling,$= p/a$ for elastic buckling
S_n	parameter of Bessel equation, defined in text
t	time
T	kinetic energy or pulse duration time
T_T	pulse time defining plastic flow solution
T_E	pulse time defining elastic, quasi-static solution
t_y	time spent in elastic motion
u	nondimensional radial displacement$= w/a$
U	strain energy of shell
U_h	strain energy of hoop mode
U_f	strain energy of flexual mode
u_c	complimentary solution of flexural mode
U_{mn}, V_{mn}, W_{mn}	modal amplitudes for axial harmonic, m and circumferential harmonic, n
$\bar{u}$	particular solution to hoop mode
V_0	initial radial velocity
v_0	nondimensional initial velocity$= \sqrt{12\rho/E_h}aV_0/h$
v	tangential displacement

vii

w	radial displacement
w_i	initial shape imperfections
w_n	natural frequency of vibration
w_y	radial motion in elastic regime
w_f	final radial motion
Z	radial inertia force
z	coordinate through shell thickness
α_n, β_n	perturbations of the initial velocity
α^2	$= \frac{h^2}{12a^2}$
β	critical damping ratio. or $= \sqrt{E_h/E}$
δ_n, γ_n	amplitudes of initial imperfections
$\overline{\delta_n}$	nondimensional initial shape imperfection $= \frac{a}{h}\delta_n$
Δ_f	$= t - t_y$
ϵ	strain
ϵ_m	strain of shell midsurface
ϵ_{mi}	midsurface strain of initial imperfections
ϵ_f	flexual strain
ϵ_y	strain at yield
$\dot{\epsilon}$	generalized strain rate
Γ_n	$= p\lambda\sqrt{1 - \lambda^2}$
γ	material viscosity constant
γ_n	perturbation amplitude of sine function
κ_I	curvature for initial shape imperfections
κ	shell curvature

λ	wave parameter $= n/s$
μ_n	parameter of Mathieu instability equation
ν	Poisson's Ratio
Ω_n	parameter of Mathieu instability equation
ϕ	angle of curvature after deformation $\frac{\partial \phi}{\partial \lambda} = \frac{1}{\rho}$
v	nondimensional tangential displacement $= v/a$, also change in shell angle of curvature, $\theta - \phi$
$1/\rho$	deformed radius of curvature
ρ	shell material density
σ_m	constant plastic flow stress
σ_H	maximum stress in hoop mode
σ_f	maximum stress in flexural mode
σ_y	yield stress
σ	generalized stress
σ_i'	deviatoric stress of component i
σ^0	current midsurface stress
σ_0	generalized stress at infinitesimally small strain rate
τ_0	termination time of elastic motion
τ	nondimensional time, defined in various sections
τ_f	time to terminal radial motion
τ_{SRR}	time at which strain rate reversal occurs
θ	circumferential coordinate, also initial angle of curvature of the shell
$\cot \gamma$	$= \beta \sqrt{(\frac{V_0/c}{\tau_y})^2 - 1}$
ζ	$= 1 - \tau/\tau_f$

1 INTRODUCTION

Buckling under static loading is traditionally investigated in the design of shell structures. Buckling instability is also a possible mode of failure in structures subject to dynamic loads. Dynamic buckling of impulsively loaded shell structures occurs through unstable growth of displacements during motion. Dynamic buckling has been considered in the design of such structures as aircraft, automobiles, trains, pipelines and reactor pressure vessels to improve their resistance to accidental impact or explosion loading. A dynamic buckling mode of failure provides a high energy-absorbing mechanism which decreases the transmitted shock to internal components or personnel. Improvement in design to resist shock loads from hostile weapons or operational conditions has been the goal of considering dynamic buckling in the design of military structures such as missiles and rockets. This study presents a review of theoretical developments in dynamic pulse buckling to delineate the physical concepts of the process. This review serves as a basis for further work in developing an understanding of dynamic buckling in the context of submarine pressure hull response to underwater shock loading.

Studies of submarine response to shock loading have concentrated on predicting the stress level and pattern resulting from complex pulse-structure interaction [1.2] and have generally not considered dynamic buckling failure which will probably occur after the material has reached its yield limit. As in static load studies, critical combinations of structural parameters and load will cause instability, and as in static analysis, detection of these dynamic stability limits requires special formulae and/or numerical methods. Previous work in dynamic buckling has been mainly for axisymmetric, pulse loading of unstiffened cylinders. The submarine problem is more complex as it requires consideration of asymmetric pulse loading of ring stiffened cylinders.

The term 'dynamic buckling' has been used to describe two different types of structural behaviour mechanisms. The first type is buckling of a structure subject to periodic loading functions which result in a resonance with a buckling mode. This is termed 'parametric buckling', as the loading function is a parameter of the displacements in the differential equation which describes the motion [3]. The load intensity to cause collapse can be lower than the static buckling load for parametric buckling behaviour. The second type of dynamic buckling is usually termed 'pulse buckling' resulting from a transient loading function of a single pulse form. Pulse loading intensities needed to cause buckling are larger than the static buckling load. This review is concerned primarily with the latter, 'pulse buckling' definiton of dynamic buckling, as it corresponds to buckling caused by shock loads.

An extensive review of the theory and analytical solutions to the pulse buckling problem is given in Section 2 for the purpose of developing an understanding of the physics of dynamic pulse buckling. The Stanford Research Institute (SRI) has devoted effort to this topic for the last three decades and most relevant work comes from this source. A collection of SRI work has been compiled in a comprehensive manuscript [4]. Other reviews of dynamic pulse buckling are given in References [5.6.7]. As is the case for theoretical studies of most complex problems,

1

analytical solutions have been derived only for relatively simple geometries and loading functions. Asymmetric loading, ring stiffeners and other con·lexities make analytical solutions for pulse buckling of submarine pressure hulls unlikely. Numerical modelling by finite element or finite difference methods offers a means of solving these more complex problems. In any type of analysis, one must know before hand what structural behaviou to expect, and formulate a model accordingly. The physics of dynamic buckling is complex, in that one may not know if the response will be elastic or plastic, of short duration or long, a..d indeed, one may also not be able to define the mode or point of failure. Therefore an understanding of the theory of dynamic buckling for simple cases is essential before undertaking more complex numerical investigations.

Section 3 of this report gives approximate formulae for the determination of critical buckling modes and critical impulse loads for dynamic buckling of simplified cases. These have resulted from assumptions made to the various theories. The effects of several shell geometry and material parameters on the critical modes and loads are investigated through these formulae.

A few studies have investigated response of shells to impulsive loading by finite element or finite difference methods. A review of some of this work is given in Section 4.

2

2 THEORETICAL REVIEW

In static, linearly elastic, bifurcation buckling, the critical load is a well defined point depending only on the structural geometry, material properties and loading distribution. In dynamic pulse buckling, the solution is for excessive growth of a particular mode or modes, rather than for specific critical points. The intensity and duration of the load affect the buckling mode as well as the total response. The response also depends on the time spent in the elastic and plastic phases of the motion.

This section reviews theories for simplified physical cases of plastic flow pulse buckling and elastic pulse buckling. All theories start with the derivation of the equations of motion for the physical problem of concern. They then proceed to the solution for the unbuckled, axisymmetric, radial hoop motion. The complimentary solution for the flexural buckling motion is then considered for initial displacement and velocity perturbations with harmonic circumferential variation. Nonlinear ordinary differential equations result, requiring numerical integration for complete solution, unless linearizing assumptions can be justified. Dynamic instability is determined by investigating the boundedness of the perturbed motion; this is the Liapunov definition of instability [8]. In all cases investigated, the nonlinear differential equations are linearized and examined qualitatively to determine their stability via exponential growth of certain critical modes.

Solutions for plastic behaviour (thick shells with small radius to thickness, a/h, ratios) and elastic behaviour (thin shells with large a/h ratios) have been derived separately [9,10] and are reviewed here to illustrate the governing physics of each case. Basic assumptions of either entirely plastic or entirely elastic behaviour are needed to permit solution. The critical radius to thickness ratio for transition from predominantly elastic to predominantly plastic response is in the range of 100 to 200 for most engineering materials. The transition is not distinct. Completely plastic behaviour can be assumed for a/h ratios below 40 and completely elastic behaviour can be assumed for a/h ratios greater than 400. Shells of intermediate a/h ratios have some combination of plastic and elastic behaviour. The magnitude of the pulse also affects the ultimate response. Solutions for intermediate a/h ratio shells require consideration of significant contributions from both elastic and plastic response, and no known analytical solutions have been derived for this case.

This section presents discussions of the individual plastic and elastic theories followed by a discussion of the work of Stuiver [11] who presents a common method of deriving both the elastic and plastic equations and shows that the plastic response has some dependency on the elastic motion. Other studies which investigate the effects of shell length, pulse duration and spacial shape, varying material properties and strain rate reversal on the shell motion and stability are then reviewed. In order to facilitate the use of the various theories in design, most authors have applied simplifying assumptions to derive approximate formulae for critical dynamic buckling modes and impulses. These are presented in Section 3 along with sample calculations using

3

these formulae for a wide range of shell parameters.

2.1 Plastic Flow Pulse Buckling

Abrahamson and Goodier [9], produced the first satisfactory solution to the dynamic pulse buckling of shells in 1962. The solution was for completely plastic response of an infinite length cylinder to a perturbed axisymmetric velocity pulse. It was limited to cylinders of smaller a/h ratios where elastic behaviour can be ignored. This is the simpler of the theories for dynamic pulse buckling and illustrates the physics of problem very well. This theoretical work was verified by considerable experimental investigation.

The basic assumption of this theory is that motion occurs entirely in the plastic material regime and that the entire shell is in a state of continuously increasing compressive plane strain with no strain rate reversal. Perturbed inextensional flexural modes are superimposed on the axisymmetric, constant compressive plastic flow stress state. The resistance of the shell to the motion comes from moments produced by a stress differential across the shell thickness as a result of the strain hardening or tangent modulus. Thus, this theory has also been called the 'tangent modulus' theory as its existence is dependent upon the material having a non-zero plastic tangent modulus.

2.1.1 Derivation of the Equation of Motion

Figure 1 illustrates the stress differential occuring in a shell perturbation (local disruption in uniform radial motion) as a result of the strain hardening modulus, E_h. This stress differential results in a bending moment:

$$M = E_h I \kappa \qquad (1)$$

where $I = \frac{1}{12} h^3$ for a unit width of shell and κ is the curvature of the shell segment, the derivation of which is given in Appendix A, and is defined as:

$$\kappa = \frac{1}{a^2} \left(\frac{\partial^2 w}{\partial \phi^2} + w \right) \qquad (2)$$

The assumption is made that the solution is for a ring or an infinite length cylinder; no end effects or biaxial stress state are included in the curvature derivation. The radius and the thickness of the shell are conservatively assumed to remain at their initial value throughout the motion. In reality, the a/h ratio of the shell will decrease with the motion making the shell more resistive to buckling. The mean circumferential hoop stress, σ_m, is assummed to be constant around the circumference and with time. In reality, σ_m will vary as the radial deflection, $w(\varphi)$, varies and more important, it will also increase due to strain hardening. The strain hardening modulus is assumed to be constant and σ_m is taken as the average stress in the post yield, plastic flow region. This assumption affects the solution by overestimating the time required

5
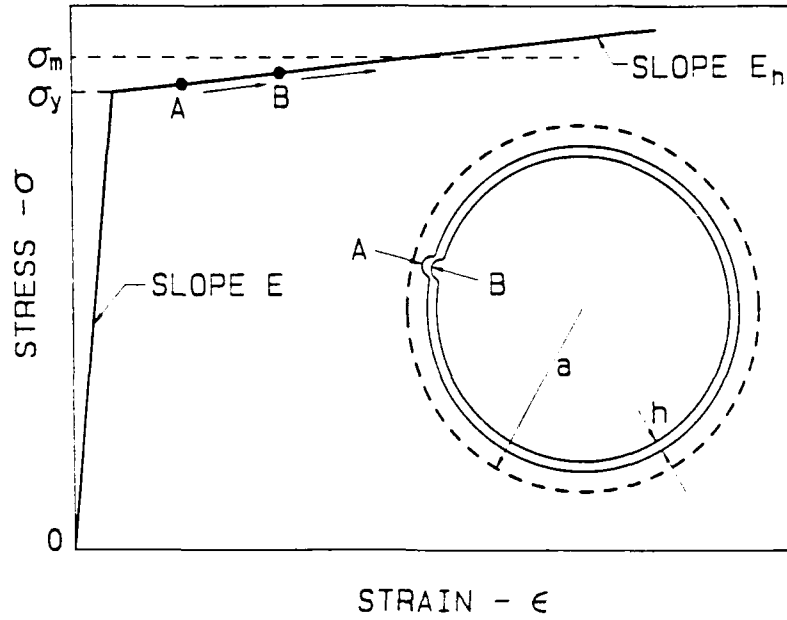
Figure 1: Strain Differential from Strain Hardening (from reference [9])

for the hoop motion to absorb the kinetic energy of the impulse. The average compressive hoop force in the shell is:

$$S = h\sigma_m \tag{3}$$

From Figure 2. equilibrium of forces results in:

$$\sum M = (M + dM)dx - Mdx - Q(d\lambda)dx = 0 \tag{4}$$

which reduces to:

$$Q = \frac{\partial M}{\partial \lambda}. \tag{5}$$

and:

$$\sum F_Z = -(Q + dQ)dx + Qdx + Zd\lambda dx - Sd\phi dx = 0 \tag{6}$$

which reduces to:

$$\frac{\partial Q}{\partial \lambda} + S\frac{\partial \phi}{\partial \lambda} = -m\frac{\partial^2 w}{\partial t^2} \tag{7}$$

where m is the mass/unit circumference and where $\frac{\partial \phi}{\partial \lambda} = \frac{1}{\rho}$ in which $\frac{1}{\rho}$ is the deformed radius of curvature defined by:

$$\frac{1}{\rho} = \frac{1}{a} + \kappa = \frac{1}{a} + \frac{1}{a^2}(\frac{\partial^2 w}{\partial \theta^2} + w). \tag{8}$$

6
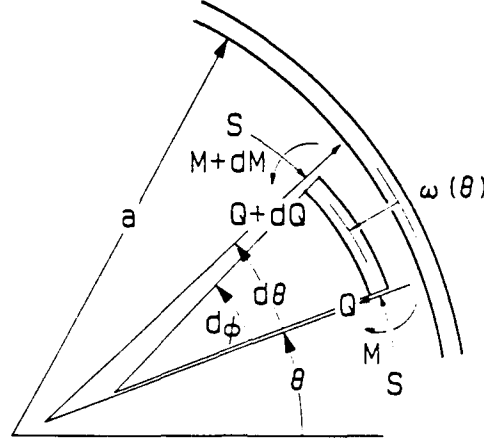
Figure 2: Shell Force Components

Substituting equations (2) and (1) into equation (5) and equations (8) and(5) into equation (7) gives the partial differential equation of motion for the shell:

$$\frac{E_h I}{a^4}\left(\frac{\partial^4 w}{\partial\theta^4} + \frac{\partial^2 w}{\partial\theta^2}\right) + S[\frac{1}{a} + \frac{1}{a^2}\left(\frac{\partial^2 w}{\partial\theta^2} + w\right)] = -m\frac{\partial^2 w}{\partial t^2}. \tag{9}$$

Reference [9] rewrites equation (9) in dimensionless form using:

$$u = \frac{w}{a}, \tau = \sqrt{\frac{E_h I}{ma^4}}t = \frac{1}{\sqrt{12}}\sqrt{\frac{E_h}{\rho}}\frac{ht}{a^2} \text{ and } s^2 = \frac{Sa^2}{E_h I} = \frac{12\sigma_m a^2}{E_h h^2} \tag{10}$$

to give equation (9) as:

$$\frac{\partial^4 u}{\partial\theta^4} + (1 + s^2)\frac{\partial^2 u}{\partial\theta^2} + s^2 u + \frac{\partial^2 u}{\partial\tau^2} = -s^2 \tag{11}$$

2.1.2 Particular Solution

The particular solution to equation (11) is for the unperturbed, axisymmetric, radial motion of the perfect ring (ie. ω is independent of θ). Equation (11) is reduced to:

$$\frac{\partial^2 u}{\partial\tau^2} + s^2 u = -s^2 \tag{12}$$

7

with initial conditions for an initial velocity pulse:

$$w(o) = u(o) = 0, \text{ and } (\frac{\partial w}{\partial t})_{t=0} = V_0, \text{ which becomes } (\frac{\partial u}{\partial \tau})_{\tau=0} = v_0 = \sqrt{\frac{12\rho}{E_k}\frac{a}{h}}V_o \quad (13)$$

and solution:

$$u_p(\tau) = -1 + \cos s\tau + \frac{v_o}{s}\sin s\tau. \quad (14)$$

The duration of the inward hoop motion is established from the particular solution by determining the time at which the radial velocity vanishes. Setting the first derivitive of equation (14) equal to zero gives:

$$\tau_f = \frac{1}{s}\arctan\frac{v_o}{s} \quad (15)$$

2.1.3 Perturbed Velocity Solution

The complimentary solution of equation (11) is derived assuming a harmonic circumferential perturbation in the initial velocity profile of the shell:

$$(\frac{\partial u}{\partial \tau})_{\tau=0} = v_o[1 + \sum_{n=2}^{\infty}(\alpha_n \cos n\theta + \beta_n \sin n\theta)] \quad (16)$$

where α_n and β_n are parameters dependent on the degree of velocity perturbation. This results in a solution of the form:

$$u(\tau) = \sum_{n=2}^{\infty}[f_n(\tau)\cos n\theta + g_n(\tau)\sin n\theta] \quad (17)$$

which after substitution into the homogeneous form of equation (11) gives:

$$n^4 f_n(\tau)\cos n\theta + n^4 g_n(\tau)\sin n\theta + (1+s^2)(-n^2 f_n(\tau)\cos n\theta - n^2 g_n(\tau)\sin n\theta)$$
$$+s^2(f_n(\tau)\cos n\theta + g_n(\tau)\sin n\theta) + \ddot{f}_n(\tau)\cos n\theta + \ddot{g}_n(\tau)\sin n\theta = 0 \quad (18)$$

yielding the ordinary differential equation:

$$\ddot{f}_n + [n^4 - n^2(1+s^2) + s^2]f_n = 0 \quad (19)$$

and a similar equation for g_n. The coefficient,

$$[n^4 - n^2(1+s^2) + s^2] = (n^2 - 1)(n^2 - s^2) = p_n^2 \quad (20)$$

determines the stability of motion. For $n < s$, f_n and g_n are hyperbolic, unstable functions and for $n > s$, f_n and g_n are circular, stable functions. In other words, only circumferential modes,

n, which are less than the shell parameter, s, will grow exponentially if the load intensity is great enough. For example, a shell of parameters a/h=30, $E_h = 10^6$ psi and σ_m=75,000 psi has a value s=29 which allows a large number of harmonics, n, to grow unbounded. One of these unbounded harmonics will predominate.

Taking the value of s to be its nearest greater integer value, the complimentary solution of f_n and g_n is:

$$f_n(\tau) = \sum_{n=2}^{n=s} (A_n \cosh p_n\tau + B_n \sinh p_n\tau)\cos n\theta + \sum_{n=s+1}^{\infty} (A_n \cos p_n\tau + B_n \sin p_n\tau)\cos n\theta \quad (21)$$

where $p_n^2 = (n^2 - 1)(s^2 - n^2)$ for $n \le s$, or, $= (n^2 - 1)(n^2 - s^2)$ for $n \ge s + 1$.

2.1.4 Complete Solution

Adding equations (21) and (14) gives the complete solution as:

$$u(\tau,\theta) = -1 + \cos s\tau + \frac{v_o}{s}\sin s\tau + \sum_{n=2}^{n=s}[(A_n \cosh p_n\tau + B_n \sinh p_n\tau)\cos n\theta$$

$$+(C_n \cosh p_n\tau + D_n \sinh p_n\tau)\sin n\theta] + \sum_{n=s+1}^{\infty}[(A_n \cos p_n\tau + B_n \sin p_n\tau)\cos n\theta$$

$$+(C_n \cos p_n\tau + D_n \sin p_n\tau)\sin n\theta] \quad (22)$$

A_n and C_n are zero from the initial conditions (13) and B_n and D_n are determined from the initial velocity perturbation. equation (16), to be: $B_n = \frac{v_o \alpha_n}{p_n}$ and $D_n = \frac{v_o \beta_n}{p_n}$ giving the final solution as:

$$u(\tau,\theta) = -1 + \cos s\tau + \frac{v_o}{s}\sin s\tau + v_o \sum_{n=2}^{n=s}(\alpha_n \cos n\theta + \beta_n \sin n\theta)\frac{1}{p_n}\sinh p_n\tau$$

$$+v_o \sum_{n=s+1}^{\infty}(\alpha_n \cos n\theta + \beta_n \sin n\theta)\frac{1}{p_n}\sin p_n\tau \quad (23)$$

The buckling instability occurs as a result of excessive growth of the $\frac{1}{p_n}\sinh p_n\tau$ term. One value of p_n will dominate the response. Taking the derivitive of $\frac{1}{p_n^2}\sinh^2 p_n\tau$ gives the limit point as:

$$(p_n^2)_{cr} = \frac{1}{4}(s^2 - 1)^2, \text{ or, } n_{cr}^2 = \frac{1}{2}(s^2 + 1) \quad (24)$$

For the shell dimensions used in the above example, $(p_n)_{cr}$ is 420 giving an n_{cr} of 21 as the critical mode for dynamic pulse buckling. The function $\frac{1}{p_n}\sinh p_n\tau$ should be investigated for a range of n in the vicinity of n_{cr}, and for a duration τ_f defined by equation (15) to determine the instability characteristics.

9

Since this theory has used the assumption of monotonically increasing compressive strain, the limit point of strain rate reversal has to be investigated. The total compressive strains consisting of the hoop strain and flexural strain for the inside and outside surfaces, respectively, are:

$$\epsilon(\tau, \theta) = [1 + \frac{h}{2a}][\frac{w}{a} + \frac{h}{2a^2}\frac{\partial^2 w}{\partial \theta^2}] \text{ and } [1 - \frac{h}{2a}][\frac{w}{a} - \frac{h}{2a^2}\frac{\partial^2 w}{\partial \theta^2}]. \tag{25}$$

These equations, upon substitution of equation (23) have to be investigated at various times throughout the motion to determine the onset of strain rate reversal. The occurrence of strain rate reversal is an indication that instability is imminent.

2.1.5 Discussion of Plastic Flow Buckling

A number of assumptions have been made in Abrahamson and Goodier's plastic flow buckling theory. They are:

1. The solution is for plane strain, and therefore an infinite cylinder or ring.

2. The loading function is a perturbed, axisymmetric, radial velocity impulse at the shell surface.

3. The solution ignores the elastic behaviour completely, and therefore is applicable to shells with small a/h ratios in which significant plastic flow will occur.

4. The radial hoop motion is assumed to occur with a constant stress value, and with constant initial values of shell thickness and radius. The tangent modulus is also assumed to be constant during the motion.

5. The stress state is one of continuously increasing compression and therefore, the theory is only applicable up to the point of strain rate reversal.

All of these assumptions have been addressed in studies subsequent to that of Abrahamson and Goodier [9], which are discussed in later sections.

Defining the velocity pulse parameters, v_o, α_n and β_n is the main difficulty in using this method to define a structure's response to a shock load. Reference [9] investigated several velocity pulse profiles and although the buckled shapes differed, the results only varied by 5 percent.

For given shell dimensions, this theory may be used to establish:

• the expected dominant mode shape of plastic pulse buckling via equation (24).

• an approximation to the duration of the response time via equation (15),and

• the motion of the shell, given the velocity pulse parameters via equation (23).

10

To determine the critical impulse for dynamic buckling, one must establish a limit point at which buckling is assumed to occur. This may be in the form of a specified amplitude as is done in Section 3 where the derivation of approximate pulse buckling formulae is discussed, or may be the point of strain rate reversal detected by equation (25). Equations (23,24,15 and 25) have been investigated via a computer program for various a/h ratios, material parameters and load amplitudes. The loading function used in the code is derived from reference [9] where a parabolic perturbation is assumed. This involves only cosine, and thus α_n terms, and is of the form:

$$\dot{u}(\theta,0) = v_o[1 - \frac{1}{20}\frac{32}{\pi^3}(\cos\theta - \frac{1}{3^3}\cos 3\theta + \frac{1}{5^3}\cos 5\theta - ...)] \tag{26}$$

The maximum perturbation is 5 percent of v_o and the $n=1$ term is irrelevent to the asymmetric buckled shape. The α_n perturbation terms are then defined as $\alpha_n = \frac{v_o 32(-1)^{n-1/2}}{20\pi^3 n^3}$, for $n = 3,5,7...$

Model	a/h	V_0(in/sec)	E_h(psi)	σ_m(psi)	n_{cr}	t_f(sec)	t_{SRR}(sec)
1	30	6,000	1,000,000	50,000	17	0.00243	0.00194
2	30	4,000	1,000,000	50,000	17	0.00175	0.00175
3	30	2,000	1,000,000	50,000	17	0.00093	none
4	30	500	1,000,000	50,000	17	0.00236	none
5	25	6,000	1,000,000	50,000	14	0.002	0.0018
6	20	6,000	1,000,000	50,000	11	0.00162	0.00146
7	15	6,000	1,000,000	50,000	9	0.00121	0.00121
8	10	6,000	1,000,000	50,000	6	0.00081	0.00081
9	30	6,000	500,000	50,000	24	0.00243	0.00194
10	30	6,000	10,000	50,000	165	0.00243	0.00194
11	30	6,000	5,000,000	50,000	8	0.00243	0.00242
12	30	6,000	1,000,000	60,000	19	0.00207	0.00165
13	30	6,000	1,000,000	70,000	20	0.0018	0.00144

Table 1: Results of Plastic Flow Theory for Various Parameters

Figures 3 and 4 illustrate the growth of various modes at several values of time during the response for models 2 and 9 of Table 1. It can be seen that the growth for several modes in the vicinity of n_{cr} is exponential with time, with the n_{cr} mode becoming dominant. Table 1 shows the critical mode, termination time, τ_f, and the time at which strain rate reversal occurs, τ_{SRR}, for several shell parameters. Model 2 (Figure 3), had $\tau_{SRR} = \tau_f$, so that the solution remains valid throughout the motion. In model 9 (Figure 4), τ_f was greater than τ_{SRR}; as a result, the solution was no longer applicable because very rapid growth occurs, as can be seen
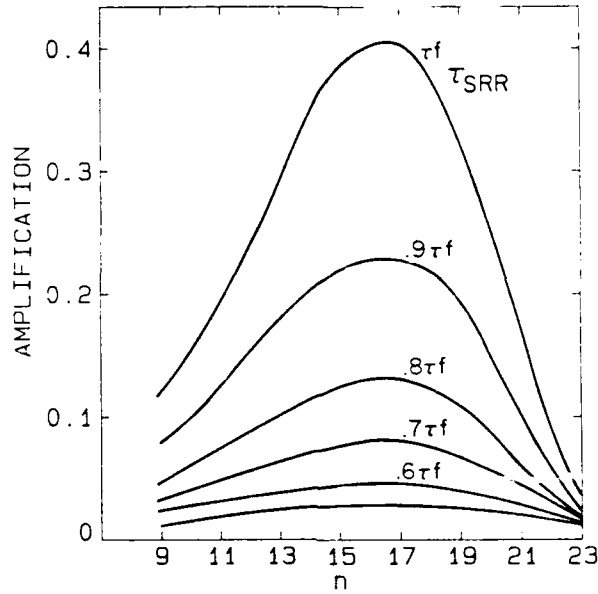
11

Figure 3: Modal Growth for Model 2

in Figure 4. Trends from Table 1 indicate that the critical mode increases with increasing a/h. decreases with increasing tangent modulus. E_h. increases with increasing flow stress. σ_{m_i}. and remains unchanged with variation in the magnitude of the initial velocity impulse. The time of terminal motion. τ_f (the time at which the shell velocity first reaches zero). is a function of the rate at which the initial energy can be absorbed by the shell. As the shell becomes thicker (lower a/h ratio). τ_f decreases and as the initial velocity (energy input) increases. τ_f increases. Abrahamson and Goodier [9] experimentally investigated the behaviour of several long cylinders and found good agreement with the theoretical mode predictions for lower a/h ratios.

Reference [12] advances the theory of reference [9] to include initial shape imperfections in the shell and the effect of increasing thickness. decreasing radius and varying material properties on the response of the cylinder. The radius is now defined as:

$$r = a - w_o \qquad (27)$$

where w_o is the uniform radial motion. This results in a redefinition of the curvature as:

$$\kappa = \frac{1}{r} - \frac{1}{a} + \frac{1}{a^2}(w + \frac{\partial^2 w}{\partial \theta^2}) \qquad (28)$$

An additional term in the curvature to include the initial imperfections is given as:

$$\kappa_i = \frac{1}{r^2}(w_i + \frac{\partial^2 w_i}{\partial \theta^2}) \qquad (29)$$

12
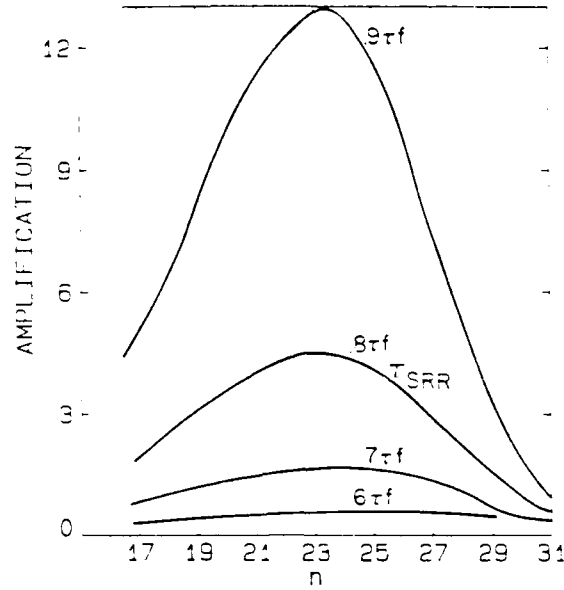
Figure 4: Modal Growth for Model 9

so that equation (8) becomes:

$$\frac{\partial \phi}{\partial \lambda} = \frac{1}{\rho} = \frac{1}{a} + \kappa + \kappa_i \qquad (30)$$

Using equations (27 to 30) in equation (7) gives the equation of motion as:

$$\frac{E_h I}{r^4}\left(\frac{\partial^4 w}{\partial \theta^4} + \frac{\partial^2 w}{\partial \theta^2}\right) + \frac{S}{r^2}\left[(w + \frac{\partial^2 w}{\partial \theta^2}) + (w_i + \frac{\partial^2 w_i}{\partial \theta^2})\right] = -m\frac{\partial^2 w}{\partial t^2} \qquad (31)$$

where h is now defined as $h_o\frac{2}{r}$.

The solution of equation (31) follows that of equation (9) except that it must be evaluated numerically if variations in E_h, σ, h and r are to be considered. This formulation has been used in reference [12] to establish critical velocities for which excessive buckling will not occur.

An independent development of the plastic flow theory is given in Section 2.3 from Reference [11] which encompasses the elastic influence on the plastic flow behaviour. The important conclusion is that as the a/h ratio becomes higher, the elastic portion of the response influences the formation of the critical mode and the ultimate motion.

13

2.2 Elastic Pulse Buckling

Goodier and McIvor [10], and Lindberg [13,4], produced a theory of elastic pulse buckling for rings and long shells subject to perturbed, axisymmetric, velocity pulses, similar to the perturbation theory for plastic flow pulse buckling. The mode formation occurs during elastic motion and the theory considers only elastic behaviour. Flexural buckling modes are assumed to form before the hoop mode reaches yield. Additional energy above that which could be absorbed elastically in the hoop mode is assumed to go into forming permanent plastic hinges in the flexural modes. For engineering materials, the elastic buckled form can occur for shells of a/h ratios greater than approximately 260. Shells with an a/h ratio below this value will have their hoop mode enter the plastic flow region before significant elastic flexural motion occurs, although the elastic motion will influence the resulting plastic flow buckling mode [11].

The mechanism of producing buckling modes is a transfer of energy from a fundamental hoop mode to flexural modes. This is also the physical mechanism for plastic flow buckling. However, in the plastic flow buckling theory, the hoop mode membrane energy is considerably greater than the energy which is transferred to flexural modes and the actual energy transfer is not considered (ie. the loss of energy from the hoop mode is neglected). In elastic pulse buckling, almost all energy can be transferred between the hoop and flexural modes. The differential equation of motion for this case is the Mathieu equation [3], which is discussed further in Appendix B. The Mathieu equation models transfer of energy from a periodic loading function to a vibratory buckling mode of one half the frequency of the driving force. Parametric instability results if sufficient energy is transferred to cause buckling. Since we are dealing with pulse loading, there is no periodic external driving frequency; however, the hoop mode oscillates at a natural frequency and energy can be transferred to a flexural mode of half of this hoop mode frequency. This is termed 'autoparametric' instability since the driving force is self generated. The main difference with the classical parametric instability is that the autoparametric instability case does not have a sustained energy input and if the shell does not buckle permanently on the first phase of the hoop motion, it will only vibrate with a continuous energy interchange between hoop and flexural modes until damping ceases the motion. The magnitude of the initial velocity in relation to the shell geometry dictates whether permanent buckling or only vibrations will occur. Even if buckling does not occur, stress values in excess of hoop mode stress values are generated by the superposition of the amplified flexural modes.

Since the coupling between hoop and flexural modes is an integral part of the motion, one mode cannot be assumed to occur independently of the other, as in the plastic flow buckling theory. In plastic flow buckling, the hoop mode thrust is assumed to remain constant until motion stops, as it is of considerably greater energy than the flexural modes. In the elastic case, the transfer of energy needs to be considered and coupling terms between the fundamental hoop mode and flexural modes have to be maintained in the solution.

14

2.2.1 Derivation of the Equation of Motion

The equation of motion in section 2.1 for plastic flow buckling was derived on equilibrium principles. For elastic pulse buckling, energy formulations and Lagrange's equation are used to derive the equation of motion [4].

The radial and tangential shell displacements with initial imperfections, are expressed as:

$$\overline{w}(\theta,t) = w(\theta,t) + w_i(\theta)$$
$$\overline{v}(\theta,t) = v(\theta,t) + v_i(\theta) \tag{32}$$

where w_i and v_i are initial imperfections and w and v are the radial and tangential displacements measured from the initial w_i, v_i state.

The kinetic energy per unit length of shell is given by:

$$T = \frac{1}{2}\rho h a \int_0^{2\pi} [(\frac{\partial w}{\partial t})^2 + (\frac{\partial v}{\partial t})^2] d\theta. \tag{33}$$

Reference [4] uses the dimensionless quantities:

$$u = \frac{u}{a}, \quad u_o = \frac{w_i}{c}, \quad v = \frac{v}{a}, \quad v_i = \frac{v_i}{a} \text{ and } \tau = \frac{ct}{a} \tag{34}$$

where $c = \sqrt{\frac{E_i}{\rho}}$ and $E_i = \frac{E}{1-\nu^2}$, to give equation (33) as:

$$T = \frac{1}{2}E_i h a \int_0^{2\pi} [(\frac{\partial u}{\partial \tau})^2 + (\frac{\partial v}{\partial \tau})^2] d\theta. \tag{35}$$

The strain energy of the shell is defined as:

$$U = \frac{E_i a}{2} \int_0^{2\pi} \int_{-h/2}^{h/2} \epsilon^2 dz\, d\theta \tag{36}$$

where the hoop stress is given by $E_i \epsilon$.

The total circumferential strain, ϵ, is the sum of the middle surface hoop strain, ϵ_m, and the flexural strain from the change in curvature a distance, z, from the middle plane:

$$\epsilon = \epsilon_m + z\kappa \tag{37}$$

which when substituted into equation (36) gives the strain energy as:

$$U = \frac{1}{2}E_i h a \int_0^{2\pi} [\epsilon_m^2 + a^2\alpha^2\kappa^2] d\theta \tag{38}$$

15

where $\alpha^2 = \frac{h^2}{12a^2}$ and κ, the curvature, is defined by equation (2) and derived in Appendix A.

Equation (38) is nonlinear and terms up to 4th order are required to maintain the required coupling of hoop and flexural modes [4].

The midsurface hoop strain is defined by a change in length of a circumferential element from $ad\theta$ to $rd\theta$ given by:

$$\epsilon_m = \frac{1}{a}[\sqrt{(\frac{\partial r}{\partial \theta})^2 + r^2(\frac{\partial \phi}{\partial \theta})^2} - 1] \tag{39}$$

which, when put in dimensionless form, and using the relations $u = a - r$ and $v = \phi - \theta$, gives, after reduction [4]:

$$\epsilon_m = \frac{\partial v}{\partial \theta} - u - u\frac{\partial v}{\partial \theta} + \frac{1}{2}(\frac{\partial u}{\partial \theta})^2 \tag{40}$$

Including initial imperfections in the midsurface strain gives: $\bar{\epsilon}_m = \epsilon_m - \epsilon_{m_i}$ which after simplification becomes:

$$\epsilon_m = \frac{\partial v}{\partial \theta} - u - \zeta\frac{\partial v}{\partial \theta} + \frac{1}{2}(\frac{\partial u}{\partial \theta})^2 + \frac{\partial u}{\partial \theta}\frac{\partial u_i}{\partial \theta} - u_i\frac{\partial v}{\partial \theta} - \zeta\frac{\partial v_i}{\partial \theta} \tag{41}$$

Substituting equations (2) and (41) into equation (38) gives the strain energy as:

$$U = \frac{1}{2}E_1 h a \int_0^{2\pi} [(\frac{\partial v}{\partial \theta} - \zeta)^2 + (\frac{\partial v}{\partial \theta} - \zeta)\{(\frac{\partial u}{\partial \theta})^2 - 2\zeta\frac{\partial v}{\partial \theta} + 2\frac{\partial u}{\partial \theta}\frac{\partial u_i}{\partial \theta}$$
$$-2u_i\frac{\partial v}{\partial \theta} - 2u\frac{\partial v_i}{\partial \theta}\} + (u\frac{\partial v}{\partial \theta} - \frac{1}{2}(\frac{\partial u}{\partial \theta})^2)^2 + \alpha^2(\frac{\partial^2 u}{\partial \theta^2} + u)]d\theta \tag{42}$$

with shape imperfections and 4th order terms maintained. The displacements are now expressed as Fourier series:

$$u(\tau, \theta) = a_0(\tau) + \sum_{n=1}^{\infty}[a_n(\tau)\cos n\theta + b_n(\tau)\sin n\theta]$$

$$v(\tau, \theta) = \sum_{n=1}^{\infty}[c_n(\tau)\cos n\theta + d_n(\tau)\sin n\theta] \tag{43}$$

Shell inextensibility is assumed, which gives: $c_n = -b_n/n$ and $d_n = a_n/n$. Imperfections are taken in the form [4]:

$$\frac{\partial v_i}{\partial \theta} = u_i = \sum_{n=2}^{\infty}[\delta_n\cos n\theta + \gamma_n\sin n\theta] \tag{44}$$

to give the energy expressions:

$$T = \pi E_1 h a[(\frac{\partial a_0}{\partial \tau})^2 + \frac{1}{2}\sum_{n=2}^{\infty}(\frac{n^2+1}{n^2})((\frac{\partial a_n}{\partial \tau})^2 + (\frac{\partial b_n}{\partial \tau})^2)] \tag{45}$$

16

and:

$$U = \pi E_l ha[a_0^2 + \frac{1}{2}\sum_{n=2}^{\infty}[(n^2-1)^2\alpha^2 - (n^2-2)a_0](a_n^2 - b_n^2)$$

$$-\frac{1}{2}\sum_{n=2}^{\infty}\frac{3}{8}(n^4 - \frac{4}{3}n^2 + 4)(a_n^4 + b_n^4) - \sum_{n=2}^{\infty}(n^2-2)(\delta_n a_n + \gamma_n b_n)a_0] \tag{46}$$

To obtain the equation of motion, equations (45) and (46) are substituted into the Lagrange equation:

$$\frac{d}{dt}(\frac{\partial T}{\partial \dot{x}_i}) - \frac{\partial T}{\partial x_i} + \frac{\partial U}{\partial x_i} = 0 \tag{47}$$

to give:

$$\ddot{a}_0 + a_0 - \frac{1}{4}(n^2-2)a_n^2 = 0, \text{ for the generalized coordinate, } x_i = a_0 \tag{48}$$

and

$$\ddot{a}_n + (w_n^2 - f_n a_0)a_n + \frac{3}{8}n^2 f_n g_n a_n^3 = \sqrt{12}\alpha f_n \overline{\delta}_n a_0, \text{ for, } x_i = a_n \tag{49}$$

where $w_n^2 = \frac{n^2(n^2-1)^2\alpha^2}{n^2+1}$, $f_n = \frac{n^2(n^2-2)}{n^2+1}$, $g_n = \frac{n^4 - \frac{4}{3}n^2 + 4}{n^2(n^2-2)}$, and the nondimensional imperfection is $\overline{\delta}_n = \frac{a}{h}\delta_n$. The b_n terms have been omitted since solution will concern only a few specific amplified harmonics and the phasing of several harmonic components will not greatly affect the solution.

2.2.2 Impulse Velocities for Vibration and No Buckling

For velocities which do not cause the shell to buckle in the first phase of the hoop mode, the shell will vibrate with energy interchanging between the hoop and flexural modes. At early motion, most of the energy will be in the hoop mode and the a_n^2 term can be neglected in equation (48) to give solution:

$$a_0 = \frac{V_0}{c}\sin\tau \tag{50}$$

for an initial axisymmetric radial velocity of V_0.

Substituting equation (50) into equation (49) and redefining parameters in the Mathieu equation format [3], gives:

$$\ddot{a}_n + (\Omega_n - \mu_n\sin\tau)a_n = \sqrt{12}\alpha\overline{\delta}_n\sin\tau \tag{51}$$

where the Mathieu stability parameters are defined as [4]:

$$\Omega_n = w_n^2 = \frac{\alpha^2 n^2(n^2-1)^2}{(n^2+1)} \tag{52}$$
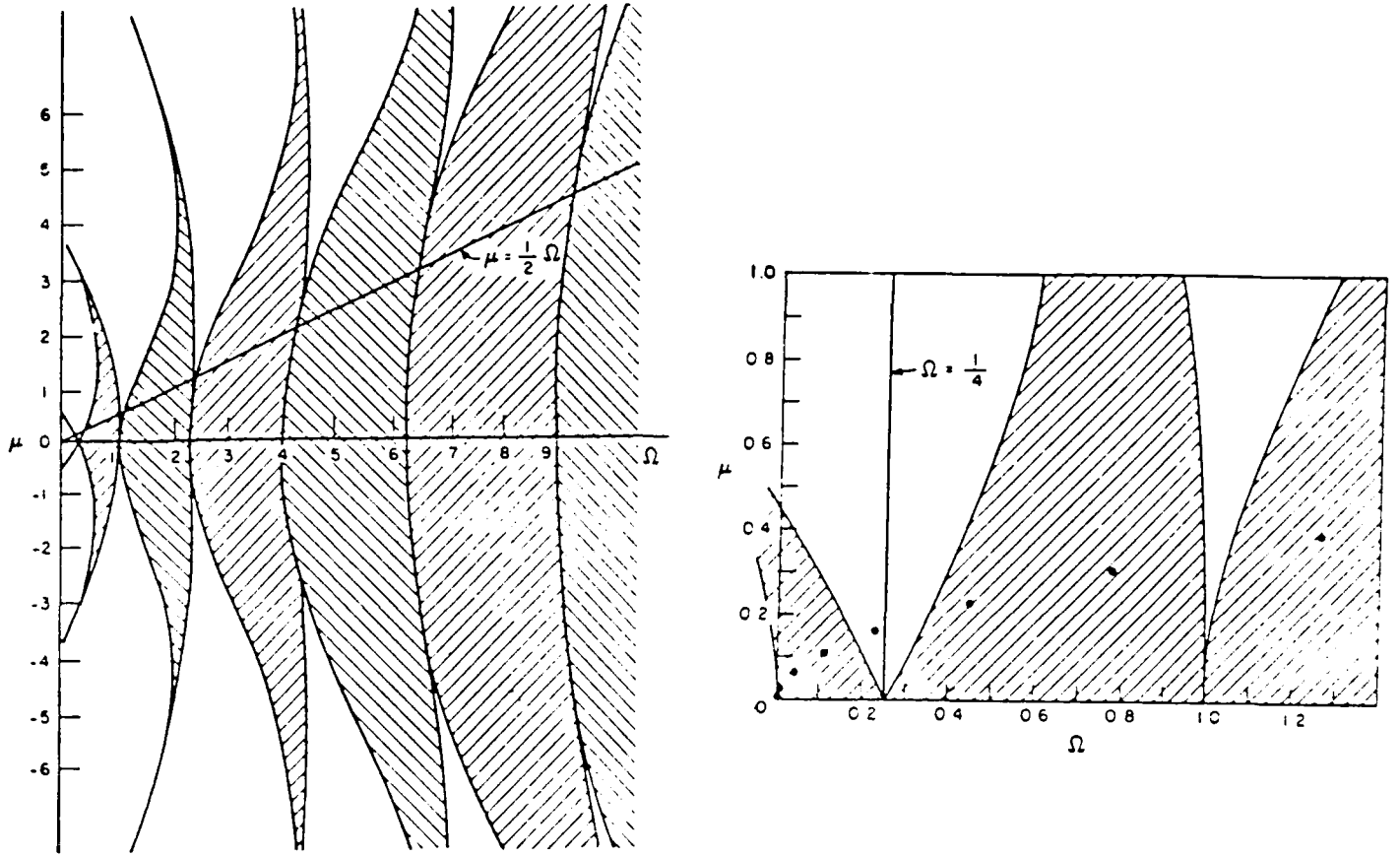
Figure 5: Mathieu Stability Diagram (from reference [10])

and:

$$\mu_n = \frac{f_n V_0}{c} = \frac{n^2(n^2 - 2)V_0}{(n^2 + 1)c} \tag{53}$$

The format of the Mathieu equation, (51), is given in a simpler homogeneous form in reference [10], where initial imperfections and fourth order terms are omitted in the strain energy expression since only small velocities are considered.

A curve of Ω_n versus μ_n, both of which are functions of the shell parameter, α, the initial velocity, V_0 and the circumferential wave number, n, can be plotted on the Mathieu stability diagram. This is shown in Figure 5. The derivation of the stability regions (shaded areas) on the Mathieu diagram is a very difficult process and is discussed further in Appendix B and reference [14].

It can be seen in Figure 5 that for this case of small initial velocity, the curve passes mainly through regions of stability with the exception of the $\Omega_n = 1/4$ abscissa which is unstable for any μ_n (with no damping). Setting $\Omega_n = 1/4$ in equation (52) gives an approximation for the

18
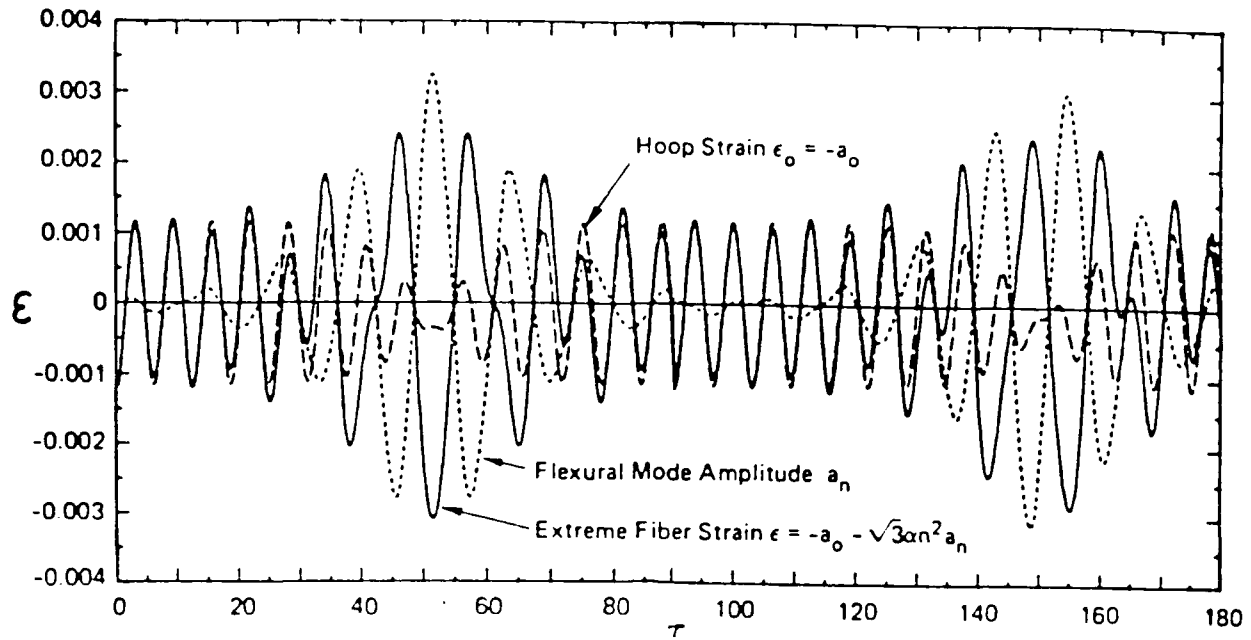
Figure 6: Response Showing Transfer of Energy From Hoop to Flexural Modes (from reference [4])

critical mode as [10]:

$$n_{cr} = 1.316\sqrt{\frac{a}{h}} \tag{54}$$

assuming $n_{cr} >> 1$. This also gives the critical frequency of w_n equal to one half of the hoop mode frequency necessary to have 'autoparametric' instability. Using the relationship $n_{cr} >> 1$, the Mathieu equation (51) can be rewritten in the form [4]:

$$\ddot{a}_n + p^2\lambda^2(\lambda^2 - \sin\tau)a_n = p^2\lambda^2\alpha\sqrt{12\delta_n}\sin\tau \tag{55}$$

with $p = \frac{\dot{v}_0}{c\alpha}$, $\lambda = \frac{n}{s}$ and $s^2 = \frac{p}{\alpha}$ from which p can be used as a 'stability' parameter in that it contains the necessary parameters, α and V_0, to establish instability from the Mathieu diagram.

The motion of the shell is determined by including the a_n^2 term in the equation of motion, (48), to allow for coupling between the hoop and flexural modes. Reference [4] omits the a_n^3 term in equation (49) and attains a solution to the shell motion by numerical integration. The results are reproduced in Figure 6. It can be seen that energy is almost completely transferred between the hoop and flexural modes.

A third curve in Figure 6 is that of the peak outer fiber strain. This is the structurally important aspect of the autoparametric behaviour for small initial velocities where permanent buckling does not occur. It can be seen that the peak strain occuring during the flexural

19

mode is considerably greater than that during the hoop mode. An analysis not considering this autoparametric effect would not detect this amplification and would underestimate the peak stress under an impulsive load.

To estimate the stress amplification from flexural vibrations, the peak hoop and flexural stresses can be derived assuming that there is complete energy transfer uniquely to both modes from the initial kinetic energy. The initial kinetic energy can be determined from equation (33) for an initial velocity. V_0, as:

$$T = \pi \rho h a V_0^2 \tag{56}$$

The strain energy of the shell, assuming that it is entirely in the hoop mode. is determined from equation (46) as:

$$U_H = \pi E_l h a a_0^2 \tag{57}$$

The strain energy assuming that it is entirely in the flexural mode. n_{cr}. is also determined from equation (46) with the additional assumptions that $n_{cr} >> 1$ and that 4th order terms are negligible. as:

$$U_f = \frac{1}{2}\pi E_l h a n_{cr}^4 a^2 a_n^2 \tag{58}$$

Equating equation (56) with equations (57) and (58) and using equation (52) with $\Omega_{n_{cr}} = 1/4$ to establish the critical mode. gives an approximation of maximum amplitudes of vibration as:

$$a_0 = \frac{V_0}{c} \text{ and } a_{n_{cr}} = \sqrt{8}\frac{V_0}{c} \tag{59}$$

for the hoop and flexural modes, respectively. This means that the flexural mode amplitude is 2.83 times the hoop mode amplitude.

To compare stress amplitudes, the maximum hoop strain of $w/a = a_0 = V_0/c$ gives the maximum hoop stress as:

$$\sigma_H = E_l \frac{V_0}{c} \tag{60}$$

The flexural strain is defined from equation (37) for the curvature as:

$$\epsilon_f = z\kappa = \frac{h}{2}(\frac{1}{a^2}\frac{\partial^2 w}{\partial \theta^2}) = \frac{h}{2a}n^2 a_{n_{cr}} = \sqrt{3}an_{cr}^2 a_{n_{cr}} \tag{61}$$

which after substitution of equation (59) and equation (52) for $\Omega_{n_{cr}} = 1/4$ gives the maximum stress in the flexural mode as:

$$\sigma_f = \sqrt{6}\frac{V_0}{c}E_l = \sqrt{6}\sigma_H \tag{62}$$

which means that the stress in the autoparametrically excited flexural mode is 2.45 times that of the hoop mode.

Goodier and McIvor [10] numerically integrated the Mathieu equation of motion, equation (55), for several a/h values and present graphical results which illustrate the energy transfer between hoop and flexural modes. The a/h values used are much lower than those for which elastic dynamic buckling could occur.

The previous determination of autoparametric response, and of stress amplification factors, has been for initial velocities such that the a_n^3 term could be neglected from equation (49) for the flexural terms of motion. Lindberg and Florence [4] show that for values of the stability parameter, $p > 1/2$, this leads to unbounded growth of displacement terms. The motion for velocities resulting in $p > 1/2$, can be determined by numerical integration of the equations of motion, (48) and (49). The effect of damping can also be considered by including β, the critical damping parameter, to give the equations of motion as:

$$\ddot{a}_0 + 2\beta\dot{a}_0 + a_0 - \frac{1}{4}(n^2 - 2)a_n^2 + 2\beta\dot{a}_0 = 0 \tag{63}$$

and

$$\ddot{a}_n + 2\beta w_n\dot{a}_n + (w_n^2 - f_n a_0)a_n + \frac{3}{8}n^2 f_n g_n a_n^3 = \sqrt{12}\alpha f_n \overline{c}_n a_0 \tag{64}$$

From results of numerical integration, it was found that the critical mode number was a function of p (ie. initial velocity for constant shell parameters). An empirical fit to results of the numerical integration gave a formula for the critical mode as [4]:

$$n_{cr}^4 = \frac{s^4}{4p^2} + (0.6)^4 s^4 \tag{65}$$

where, from equation (55), $s^2 = \frac{p}{\alpha}$.

From results of the numerical integration, motions for two different values of p are shown in Figure 7. It can be seen that energy transfer to the flexural mode is complete closer to the first inward hoop motion as p increases.

To derive an expression for stress amplification similar to equation (62) for the small initial velocity case, the total energy of the system including the 4th order, a_n^4 terms, is used [4]:

$$\frac{2[U + T]}{\pi E_l h a} = 2\dot{a}_0^2 + \dot{a}_n^2 + 2a_0^2 + (n^4\alpha^2 - n^2 a_0)a_n^2 + \frac{3}{16}n^4 a_n^4 = 2p^2\alpha^2 \tag{66}$$

In determining the maximum flexural stress, it is also necessary to consider the coincident energy in the hoop mode, arising from the coupling term, $(n^4\alpha^2 - n^2 a_0)a_n^2$, in equation (66). To determine the maximum amplitude of a_0 at the point of maximum a_n, the velocities, $\dot{a}_0$ and $\dot{a}_n$ are set to zero and a_n^2 is maximized with respect to a_0. The upper bound to the stress amplification is given as:

$$\frac{\sigma_f}{\sigma_H} = A_{n_{cr}} + \frac{(A_{n_{cr}})^2}{12\lambda^2}, \text{ where, } A_{n_{cr}} = 2\sqrt{3}\lambda\sqrt{\sqrt{4\lambda^4 + 2} - 2\lambda^2} \tag{67}$$

21
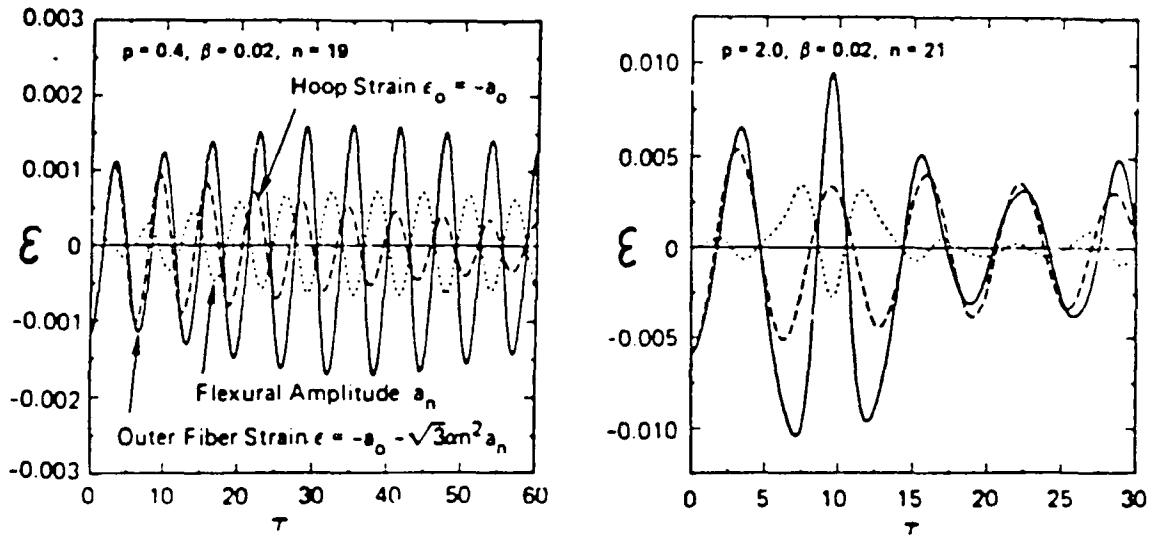
Figure 7: Elastic Motion for Various Stability Parameters, p (from reference [4])

which is shown to have values in the range of 2.5. Results from numerical integration gave stress amplification values in the order of 1.65 for $p > 1.5$ indicating that the upper bound of equation (67) may be too high [4].

2.2.3 Pulse Buckling from Large Initial Velocities

For larger initial velocities, V_0, in relation to the shell parameter, α, (ie. large p), the shell will buckle during the first compressive hoop mode. For large values of p, the curves of Ω versus μ on the Mathieu diagram (Figure 8) do not pass primarily through stable regions as was the case for smaller p values, as was shown in Figure 5. As was the case in plastic flow buckling, many modes are amplified, with one mode being dominant. In considering the Mathieu equation, (55), it is clear that the coefficient of a_n must be negative for unbounded growth. Following the approach of plastic flow buckling, the largest n for which unbounded growth may occur can be estimated by taking $\sin \tau = 1$ in equation (55), to give:

$$\lambda^2 \le 1, \ n_{max}^2 = s^2 = \frac{V_0}{c\alpha^2} \tag{68}$$

Reference [13] rewrites the Mathieu equation, (55), without initial shape imperfections as:

$$\ddot{a}_\lambda - p^2\lambda^2(\sin \tau - \lambda^2)a_\lambda = 0 \tag{69}$$

22
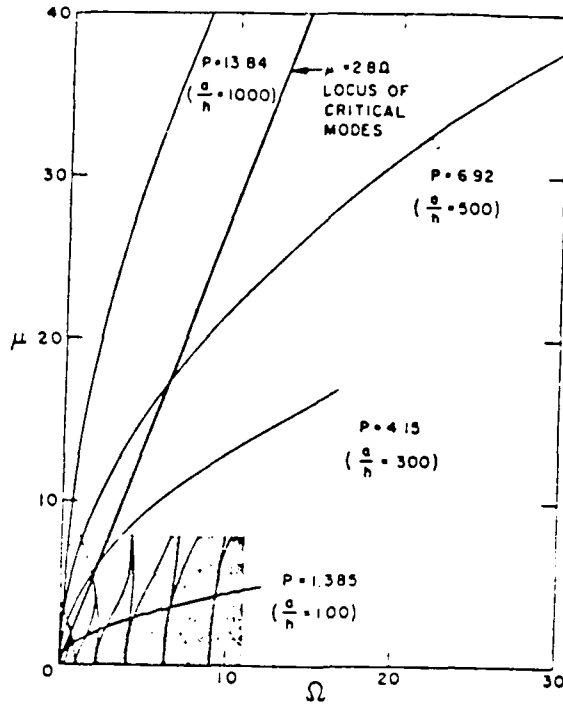
Figure 8: Mathieu Stability Diagram for Large Initial Velocities Causing Buckling (from reference [13])

with initial conditions:

$$\dot{a}_n(0) = \frac{V_0 \gamma_n}{c}, \quad a_n(0) = 0 \tag{70}$$

where γ_n are harmonic perturbations of the initial velocity field, V_0. The investigation of modal growth can be accomplished by numerical integration of equation (69) with variations in the parameters λ and p. Figure 9 shows the mode amplifications with time of an aluminum cylinder of a/h=480 and $V_0 = 800 in/sec$ [13]. It should be noted that buckling occurs for the elastic case at very high wave numbers, in the range of $n =45$ to 65.

For complete analysis of the motion of the elastic shells, equations (48) and (49) need to be numerically integrated with the initial conditions of equations (70). An empirical fit to results obtained in this manner gives a relation for the amplitude of the most amplified mode in relation to the initial imperfection as a function of the parameter, p, as [4]:

$$\frac{a_n}{\delta_n}\Big|_{max} = 1.2 e^p \tag{71}$$

The mode of maximum amplification can be estimated by solving equation (69) for a constant hoop thrust case (ie. letting $\sin \tau = 1$). This is the same assumption as is made in plastic flow buckling, where the time dependent coupling between hoop and flexural modes is

23
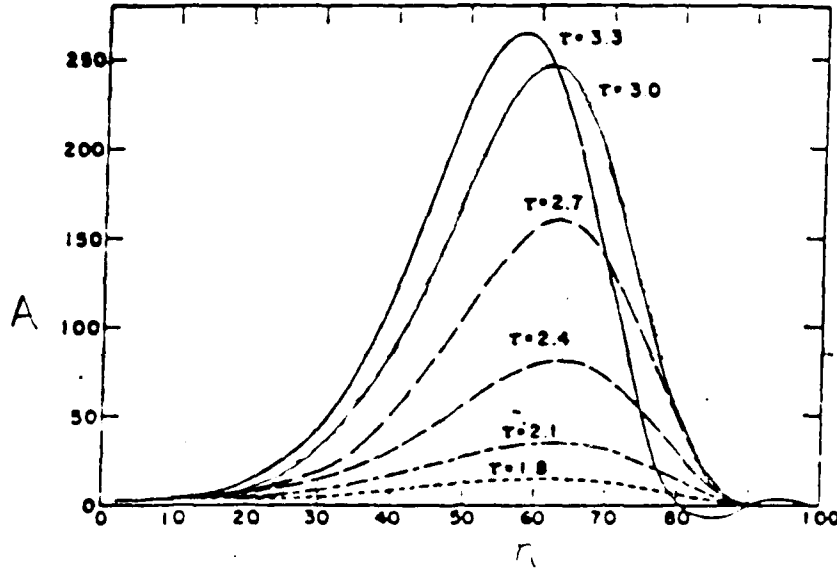
Figure 9: Modal Amplification for Elastic Dynamic Buckling of Thin Walled Cylinder (from reference [13])

neglected. This gives [13]:

$$a_\lambda(\tau) = \frac{V_0 \lambda_n}{c} \frac{\sinh \Gamma_n \tau}{\Gamma_n}, \text{ where } \Gamma_n = p\lambda\sqrt{1 - \lambda^2} \tag{72}$$

from which the maximum amplified mode can be determined by minimizing equation (72) with respect to λ to give:

$$\lambda_{cr} = \frac{1}{\sqrt{2}} \tag{73}$$

To establish whether elastic, dynamic buckling will occur for a given velocity pulse on a given shell, it is necessary to determine if either hoop or flexural yielding occur and which will occur first. Elastic, dynamic buckling is signified if flexural yield is reached first, otherwise the shell will enter the plastic flow hoop mode where dynamic buckling will occur as plastic flow buckling influenced by the elastic mode. Using equation (61) for flexural strain and equation(71) for maximum amplitude, the flexural strain can be expressed as:

$$\epsilon_f = \sqrt{3}\lambda^2 p(1.2\overline{\delta_n}\epsilon^p)\frac{h}{a} \tag{74}$$

Setting expression (74) equal to the yield strain ϵ_y gives a relation between p and h/a. A similar

24
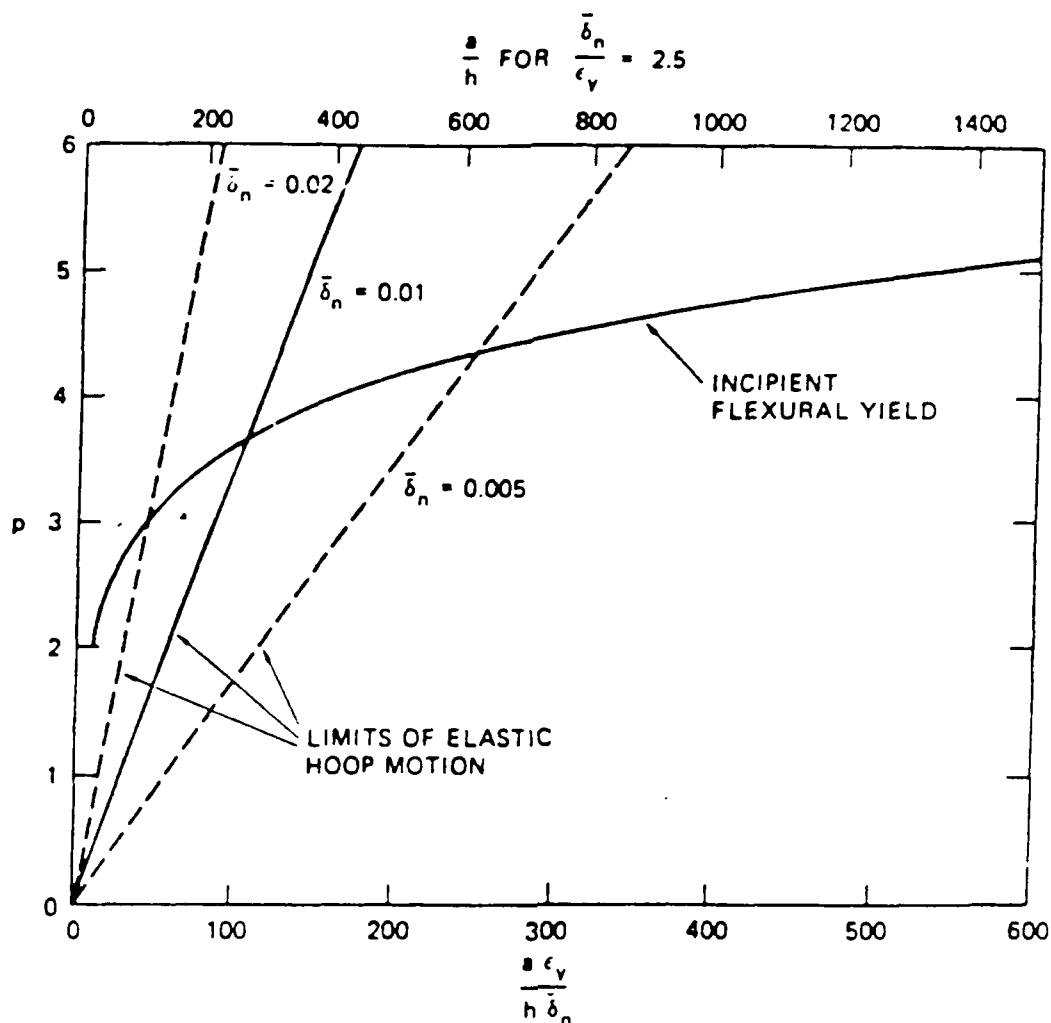
Figure 10: Hoop and Flexural Yield and Dynamic Buckling Limits for Elastic Response to Pulse Loads (from reference [4])

expression for the hoop strain can be attained by setting:

$$\frac{V_0}{c} = \frac{ph}{\sqrt{12}a} = \epsilon_y \tag{75}$$

Using the value of $\lambda_{cr} = 0.6$, from results of numerical integration of equation (69), Lindberg and Florence [4] present a curve, Figure 10, for different imperfection values, $\bar{\delta}_n$, giving hoop and flexural yield limits as functions of p and α. For practical values of initial imperfection of 1 percent of the shell thickness ($\bar{\delta} = .01$) and $\epsilon_y = .004$, it can be seen that purely elastic, dynamic buckling will not occur for shells below a/h=260. The stability parameter, p, must also be greater than 3.66 for buckling to occur, otherwise only autoparametric vibrations will occur. These parameters represent a very thin shell, thinner than would be used in most submarine applications.

The topic of autoparametric, dynamic, elastic buckling has been addressed subsequent to reference [10] by other authors. Hubka [1], derives an analytical solution to the coupled non-

25

linear differential equations of motion for response to small initial velocities. The solution agrees with the numerical results of reference [10] showing a slowly varying hoop mode function modulating a rapidly varying flexural mode.

The Mathieu type instability describes response for periodic type loadings and many references examine this [15,16,17]. This is not pursued further here as response to single pulse loading is of primary interest.

2.3 Elastic and Plastic Pulse Buckling

This section presents an analytical investigation [11] which includes both the plastic and elastic regimes in a single theory. The theory reduces to the plastic flow or elastic theories discussed in the previous two sections for limiting cases. The necessity of combining both elastic and plastic behaviour for a wide range of a/h ratios is demonstrated. Although equations of motion are produced, a general solution to the elastic-plastic case is not formulated.

The problem considered here is again for a ring or infinite shell subject to a perturbed, nearly uniform, axisymmetric velocity pulse. The linearized equation of motion, derived from equilibrium of a shell segment (see equation 7) is, with the additional assumption that u is much less than 1:

$$u^{iv} + (1 + \frac{\sigma/E}{\alpha^2\beta^2})u'' + \frac{\ddot{u}}{\alpha^2\beta^2} + \frac{\sigma/E}{\alpha^2\beta^2} = 0 \qquad (76)$$

where $\beta^2 = \frac{E_h}{E}$ and $,''$, is the spatial derivitive with respect to θ. The parameter β, in this form of the equation of motion, can be used for the elastic as well as the plastic flow case. For purely linear, elastic response, $\beta = 1$ and $\sigma/E = \epsilon$. Reference [11] considers only material of bilinear stress-strain curves represented by:

$$\sigma/E = \epsilon, \beta^2 = 1, \text{ for } 0 \leq \epsilon \leq \epsilon_y$$

$$\sigma/E = (1 - \beta^2)\epsilon_y + \beta^2\epsilon, \beta^2 = \frac{E_h}{E}, \text{ for } \epsilon_y \leq \epsilon \qquad (77)$$

Equation (76) is then divided into two regimes, one for elastic strain:

$$u^{iv} + (1 + \frac{\epsilon}{\alpha^2})u'' + \frac{\ddot{u}}{\alpha^2} + \frac{\epsilon}{\alpha^2} = 0, \text{ for } 0 \leq \epsilon \leq \epsilon_y \qquad (78)$$

and one for plastic strain:

$$u^{iv} + (1 + \frac{1 - \beta^2}{\beta^2}\frac{\epsilon_y}{\alpha^2})u'' + \frac{\ddot{u}}{\alpha^2\beta^2} + \frac{\epsilon}{\alpha^2} + \frac{1 - \beta^2}{\beta^2}\frac{\epsilon_y}{\alpha^2} = 0, \text{ for } \epsilon_y \leq \epsilon \qquad (79)$$

The initial conditions, as in the plastic and elastic cases, incorporate imperfections in the initial displacement and velocity fields, defined by the series:

$$u_0(\theta) = \frac{V_0}{c}\sum_{n=1}^{\infty}(a_{n0}\sin n\theta + b_{n0}\cos n\theta)$$

$$\dot{u}_0(\theta) = \frac{V_0}{c}[1 + \sum_{n=1}^{\infty}(a_{ni}\sin n\theta + b_{ni}\cos n\theta)] \qquad (80)$$

where a_{ni} are of perturbation order $(<<1)$.

27

The solution follows that of the previous cases, with a particular, unperturbed solution and a perturbed, complimentary solution yielding buckling terms.

Solving equations (78) and (79) for perfectly radial motion (no dependence on θ), yields the particular solutions:

$$\overline{u} = \frac{V_0}{c} \sin \tau, \text{ for } \frac{V_0}{c} = u \le \epsilon_y \tag{81}$$

and:

$$\overline{u} = -\frac{1 - \beta^2}{\beta^2} \epsilon_y + \frac{\epsilon_y}{\beta} \sqrt{\frac{1 - \beta^2}{\beta^2} + (\frac{V_0/c}{\epsilon_y})^2} \sin(\beta(\tau - \tau_0) + \varphi), \text{ for } \frac{V_0}{c} > \epsilon_y \tag{82}$$

where $\tau_0 = \arcsin \frac{\epsilon_y}{V_0/c}$, $\cot \varphi = \beta \sqrt{(\frac{V_0/c}{\epsilon_y})^2 - 1}$ and the constants of integration were derived from the initial conditions:

$$\overline{u}(\tau_0) = \frac{V_0}{c} \sin \tau_0 = \epsilon_y, \text{ and } \dot{\overline{u}}(\tau_0) = \frac{V_0}{c} \cos \tau_0 \tag{83}$$

If the initial velocity is great enough to cause $V_0/c > \epsilon_y$, then the radial hoop motion ceases at time:

$$\tau_f = \tau_0 + \frac{\pi/2 - \varphi}{\beta}. \tag{84}$$

The complimentary solutions are obtained by solving equations (78) and (79) subject to initial conditions (80). The flexural motion of the shell is assumed to be inextensional, allowing $\epsilon = \overline{u}$, and the complete solution to be taken as $u(\theta, \tau) = \overline{u}(\tau) + u_c(\theta, \tau)$. Equations (78) and (79), reduce to the variational equations of the perturbation of $\overline{u}$:

$$u_c^{iv} + (1 + \frac{\overline{u}}{\alpha^2})u_c'' + \frac{\ddot{u}_c}{\alpha^2} = 0 \text{ for } 0 \le \overline{u} \le \epsilon_y \tag{85}$$

and:

$$u_c^{iv} + [(1 + \frac{1 - \beta^2}{\beta^2} \frac{\epsilon_y}{\alpha^2}) + \frac{\overline{u}}{\alpha^2}]u_c'' + \frac{\ddot{u}_c}{\alpha^2 \beta^2} = 0 \text{ for } \epsilon_y \le \overline{u} \tag{86}$$

for which solutions of the form:

$$u_c(\theta, \tau) = \frac{V_c}{c} \sum_{n=1}^{\infty} [a_n(\tau) \sin n\theta + b_n(\tau) \cos n\theta] \tag{87}$$

are assumed.

Substitution of equation (87) into equations (85) and (86) produces the homogeneous form of the Mathieu differential equation,(51), of the elastic theory (section 2.2), if $n << 1$:

$$\ddot{q}_n + \alpha^2(n^4 - n^2 \frac{V_0/c}{\alpha^2} \sin \tau)q_n = 0, \text{ for } 0 \le \overline{u} \le \epsilon_y \tag{88}$$

28

and of the plastic regime:

$$\ddot{g}_n + \alpha^2 \beta^2 \{ n^4 - \frac{n^2}{\beta} \frac{V_0/c}{\alpha^2} \sqrt{1 + \frac{1-\beta^2}{\beta^2} (\frac{\epsilon_y}{V_0/c})^2} \sin[\beta(\tau - \tau_0) + \varphi] \} g_n = 0, \text{ for } \epsilon_y \leq \bar{u} \qquad (89)$$

the latter of which reduces to :

$$\ddot{g}_n + \alpha^2 \beta^2 [n^4 - n^2 \frac{\sigma_y}{\alpha^2 E_h}] g_n = 0, \text{ for } \beta^2 \ll 1 \qquad (90)$$

Equation (90) is similar to equation (19) of the plastic flow theory (section 2.1). Equation (89) reduces to equation (88) for elastic motion where $\beta = 1$.

Both equation (88) for the elastic case and equation (89) for the plastic flow case, are of the Mathieu instability type. Values of the parameters, n, α^2, V_0, c and β can be found which fall within the unstable regions of the Mathieu diagram. If the hoop mode response remains completely elastic (ie. $V_0 \leq c\epsilon_y$), then the mode of buckling will be established solely by equation (88) as was given in section 2.2 from Lindberg and Florence [4]. If $V_0 > c\epsilon_y$, then the hoop mode enters the plastic material regime and the buckling mode shape will be some combination of the two predominant harmonics determined from the elastic and plastic solutions. If $V_0 \gg c\epsilon_y$, then the response will be governed by the predominant mode of the plastic flow regime as was the case in section 2.1.

To obtain the predominant harmonics of equations (88) and (89). these Mathieu equations must be solved. This is of extreme analytical complexity [14]. Stuiver [11], produces an approximate solution resulting in:

$$\lambda_{el} = \frac{n_{el}}{s} = [\frac{1}{8}(1 - \frac{4}{p^4})]^{1/4} \qquad (91)$$

for the elastic regime, where λ, p and s are defined in equation (55) and:

$$n_{pl} = 0.85\sqrt{6} \frac{a}{h} (\frac{\sigma_y}{E_h})^{1/2} [1 + (.3 \frac{V_0/c}{\epsilon_y})^2]^{1/4} \qquad (92)$$

for the plastic regime. For $p > 2$, λ_{el} is equal to 0.595 which is in good agreement with the value of $\lambda_{el} = 0.6$ obtained through numerical integration [4]. Equation (92), for the plastic flow wave number, n_{pl}, gives comparable values to equation (24) of the plastic flow case derived by Abrahamson and Goodier [9].

Comparison of resultant buckled wave numbers from tests on cylinders with $9 < a/h < 36$ show that the experimental values lie between the n_{el} and n_{pl} values of equations (91) and (92) with no particularly good agreement with either value. Stuiver postulates that this is a result of both the elastic and plastic modes influencing the response.

29

A complete solution to the nonlinear differential equations describing the radial motion would be very complex and would be better left to approximate numerical methods, such as finite difference or finite element.

One such study, using a dynamic elastic-plastic, geometrically nonlinear finite difference code for rings, is presented by Wesenberg [18]. Three cylindrical shells of a/h=100, 200 and 300 were subjected to axisymmetric impulse loads, and response was measured by high speed photography. Initial imperfections were measured for the predominant resultant mode and incorporated in the finite difference solution. The radial velocity perturbations were measured from the photographs and used as the velocity perturbation parameters in the finite difference solution. The numerical solution allowed the shells to buckle, deform plastically and damp out to a final deformed shape. The permanent peak deformations for a range of impulse loads were in good agreement with the finite difference predictions. The wave number of predominant response was shown to increase linearly with the magnitude of the applied impulse. All three shells buckled in wave numbers ranging from $30 \leq n \leq 35$; however, the solution does require imperfection and perturbation input from the buckled shell which one would normally not know apriori.

Using equations (91) and (92) for the experimental aluminum shell described in reference 11, with parameters: h=0.02 in, a=2.0 in, E=10,000,000 psi, E_h=130,000 psi, $\sigma(0.2\%)$=44,000 psi, $\rho = 0.27 \times 10^{-3}$ lb-sec^2/in^4, c=200,000 in/sec and V_0=805 in/sec. gives $n_{el} = 13$ and $n_{pl} = 121$. This shell buckled experimentally at $n = 30$ [18]. This indicates that the actual response is somewhere in between the cases of purely elastic and purely plastic response for a shell of a/h=100. The plastic theory greatly overestimates the mode of fundamental response. Since both n_{el} and n_{pl} are linear functions of a/h, for the same velocity impulse, the shell with a/h=200 will have $n_{el} = 26$ and $n_{pl} = 242$ as predictions and the a/h=300 shell will have $n_{el} = 39$ and $n_{pl} = 363$ as predictions. For these thinner shells, which buckled experimentally at n=32 and n=33, respectively, the elastic prediction is in reasonable agreement. This could be expected as these shells are in the range of the elastic limit of a/h>260 reported by Lindberg and Florence [4].

2.4 Pulse Buckling for Finite Length Cylinders

The theories presented in the previous sections of this chapter have dealt with rings or long shells for which plane strain conditions have been assumed. This section discusses theory for the dynamic buckling of axisymmetrically loaded shells of finite length where biaxial stress states and end conditions have been included. First, the extension of the plastic flow buckling case to include a biaxial stress state will be discussed. Then, the elastic dynamic buckling case is considered for finite length cylinders with simply supported end conditions. Elastic dynamic buckling, particularly if the loading function is of longer duration than a pure impulse, may occur at circumferential wave numbers of small enough value that end conditions affect the response of the entire shell [19].

2.4.1 Plastic Flow Buckling of Finite Length Cylinders

As was the case in section 2.1 for rings or long cylinders, the theory derived for finite length cylinders is for the specific case of a perturbed, axisymmetric, velocity pulse on an imperfect cylinder. The theory is most applicable to thick shells ($a/h < 40$), where the hoop membrane strain will undergo significant plastic deformation before buckling occurs and elastic behaviour can be neglected. The assumption of no occurrence of strain rate reversal is also made and a linear strain hardening modulus is used as the constitutive relationship. Florence and Vaughan [20], first developed the theory for short shells with a plane stress assumption, and then extended it to consider shells of variable length to the limit of the infinite length, plane strain case [21]. The solutions are for the unbounded amplification with time, of the predominant circumferential buckling mode.

Due to the biaxial stress state, an additional resisting moment to the strain-hardening moment derived in section 2.1 exists. Material incompressibility is assumed giving the condition (in terms of strain rates):

$$\dot{\epsilon}_r + \dot{\epsilon}_\theta + \dot{\epsilon}_z = 0 \qquad (93)$$

where $\dot{\epsilon}_r = \frac{d\epsilon_r}{dt}$. The generalized strain rate and stress are defined by [20,22]:

$$\dot{\epsilon}^2 = \frac{2}{3}(\dot{\epsilon}_r^2 + \dot{\epsilon}_\theta^2 + \dot{\epsilon}_z^2) \qquad (94)$$

and:

$$\sigma^2 = \frac{3}{2}(\sigma_z'^2 + \sigma_\theta'^2 + \sigma_r'^2) \qquad (95)$$

where σ_i' are the deviatoric stress components. With the assumption of $\sigma_z = 0$ (stress through the shell thickness), and using the Levy-Mises flow law [22], $\dot{\epsilon}_i/\sigma_i' = \lambda$, where $\lambda = 3\dot{\epsilon}/2\sigma$, from equations (94) and (95), the stress components become:

$$\sigma_r = \frac{2\sigma}{3\dot{\epsilon}}(2\dot{\epsilon}_r + \dot{\epsilon}_\theta), \text{ and, } \sigma_\theta = \frac{2\sigma}{3\dot{\epsilon}}(\dot{\epsilon}_r + 2\dot{\epsilon}_\theta) \qquad (96)$$

31

and for a linear strain hardening assumption, $\dot{\sigma} = E_h \dot{\epsilon}$, which allows:

$$\sigma = \sigma_y + E_h \epsilon \tag{97}$$

where σ_y is the yield stress.

For unperturbed, radial, hoop motion, the circumferential strain rate is:

$$\dot{\epsilon}_\theta = -(1 - z/a)(\dot{w}_0/a) \tag{98}$$

where z is measured from the shell midsurface and $\dot{w}_0$ is the radial hoop motion.

With the assumption of plane stress, $\sigma_r = \sigma_z = 0$, and $\dot{\epsilon}_r = \dot{\epsilon}_z = -\dot{\epsilon}_\theta/2$ from equation (96), at the midsurface, equation (98) gives $\dot{\epsilon}_r = \dot{\epsilon}_z = \dot{w}_0/2a$. The strain rates at any point z, in the shell are defined as:

$$\dot{\epsilon}_r = \dot{w}_0/2a, \quad \dot{\epsilon}_\theta = -(1 - z/a)(\dot{w}_0/a), \quad \text{and,} \quad \dot{\epsilon}_z = -(1/2 - z/a)(\dot{w}_0/a) \tag{99}$$

which, when substituted into equation (94), with (z/a) terms of order two or more neglected, gives the generalized strain rate:

$$\dot{\epsilon} = -(1 - z/a)(\dot{w}_0/a) \tag{100}$$

and the stress relations:

$$\sigma_r = (2z/3a)\sigma \quad \text{and} \quad \sigma_\theta = -(1 - z/3a)\sigma \tag{101}$$

where the generalized stress is now defined as:

$$\sigma = \sigma_y + E_h(1 - z/a)(w_0/a) \tag{102}$$

Reference [20] defines σ^0 as the current midsurface stress:

$$\sigma^0 = \sigma_y + E_h(w_0/a) \tag{103}$$

allowing the stress components to be defined as:

$$\sigma_r = (2z/3a)\sigma^0 \quad \text{and} \quad \sigma_\theta = -\sigma^0 + (z/3a)(\sigma_y + 4E_h w_0/a) \tag{104}$$

again with z/a terms of order two or greater neglected.

The moments and membrane forces for a shell segment, determined using equation (104) are:

$$M_r = \int_{-h/2}^{h/2} \sigma_r z \, dz = (h^3/18a)\sigma^0 \tag{105}$$

32

$$M_\theta = \int_{-h/2}^{h/2} \sigma_\theta z dz = (h^3/36a)(\sigma^0 + 3E_h w_0/a) \tag{106}$$

$$N_x = \int_{-h/2}^{h/2} \sigma_x dz = 0 \text{ and } N_\theta = \int_{-h/2}^{h/2} \sigma_\theta dz = -\sigma^0 h \tag{107}$$

The equation of motion for the unperturbed state, from Figure 2 and equation (7), is:

$$N_\theta = a\rho h \frac{\partial^2 w_0}{\partial t^2} \tag{108}$$

which becomes:

$$\frac{\partial^2 w_0}{\partial t^2} + (c_h/a)^2 w_0 = -\sigma_y/a\rho \tag{109}$$

upon substitution of equations (107) and (103) and defining $c_h^2 = E_h/\rho$. For initial velocity pulse conditions, $w_0(0) = 0$ and $\dot{w}_0(0) = V_0$, the particular solution for this problem is:

$$w_0(t) = V_0(a/c_h)\sin(c_h t/a) - (\sigma_y a/E_h)[1 - \cos(c_h t/a)] \tag{110}$$

The perturbed solution is defined as $w(\theta, t)$ with the total solution being $w_0(t) + w(\theta, t)$. The curvature, from equation (8), is defined as:

$$\kappa = \frac{1}{a} + \frac{(w_0 + w)}{a^2} + \frac{1}{a^2}\frac{\partial^2 w}{\partial \theta^2} \tag{111}$$

giving the perturbed motion strain rate components as:

$$
\begin{aligned}
\dot{\epsilon}_\theta &= -(1 - z/a)\left(\frac{w_0 + w}{a}\right)^{\cdot} + \frac{z}{a^2}\frac{\partial^2 \dot{w}}{\partial \theta^2} \\
\dot{\epsilon}_x &= \frac{(w_0 + w)^{\cdot}}{2a} \\
\dot{\epsilon}_z &= (1/2 - z/a)\left(\frac{w_0 + w}{a}\right)^{\cdot} + \frac{z}{a^2}\frac{\partial^2 \dot{w}}{\partial \theta^2}
\end{aligned}
\tag{112}
$$

The generalized strain rate ,from equation (94), becomes:

$$\dot{\epsilon} = \left(\frac{w_0 + w}{a}\right)^{\cdot} - \frac{z}{a^2}\left(w_0 + w + \frac{\partial^2 w}{\partial \theta^2}\right) \tag{113}$$

with orders of z/a greater than one and perturbation products neglected. Equation (113) is integrated to give the generalized strain:

$$\epsilon = \frac{w_0}{a} + \frac{w}{a} - \frac{w_i}{a} - \frac{z}{a^2}\left[w_0 + (w - w_i) + \frac{\partial^2(w - w_i)}{\partial \theta^2}\right] \tag{114}$$

33

where w_i is defined in reference [20] as the initial deformed shape, $w_i = w(\theta, 0)$. The generalized stress is then given as:

$$\sigma = \sigma^0 + \frac{E_h}{a}(w - w_i) - \frac{E_h z}{a^2}[w_0 + (w - w_i) + \frac{\partial^2(w - w_i)}{\partial\theta^2}] \tag{115}$$

Equations (96),(112) and (115) and a binomial expansion of equation (113), give stress components:

$$\sigma_x = \frac{2z}{3a}[\sigma^0(1 + \frac{1}{\dot{w}_0}\frac{\partial^2 w}{\partial\theta^2}) + \frac{E_h}{a}(w - w_i)] \tag{116}$$

$$\sigma_\theta = -[\sigma^0 + \frac{E_h}{a}(w - w_i)] + \frac{z}{3a}[\sigma^0(1 + \frac{1}{\dot{w}_0}\frac{\partial^2 w}{\partial\theta^2}) + \frac{E_h}{a}(3w_0 + 4(w - w_i) + 3\frac{\partial^2(w - w_i)}{\partial\theta^2}]$$

with resultant moments and membrane forces:

$$M_x = \frac{h^3}{18a}[\sigma^0(1 + \frac{1}{\dot{w}_0}\frac{\partial^2 w}{\partial\theta^2}) + \frac{E_h}{a}(w - w_i)] \tag{117}$$

$$M_\theta = \frac{h^3}{36a}[\sigma^0(1 + \frac{1}{\dot{w}_0}\frac{\partial^2 w}{\partial\theta^2}) + \frac{E_h}{a}(3w_0 + 4(w - w_i) + 3\frac{\partial^2(w - w_i)}{\partial\theta^2})] \tag{118}$$

$$N_x = 0 \text{ and } N_\theta = -h[\sigma^0 + \frac{E_h}{a}(w - w_i)] \tag{119}$$

The second term of M_θ in equation (118) is the resisting moment from strain hardening, E_h, which governed the theory of section 2.1 for infinite shells. The first term of M_θ, $\frac{h^3}{36a}\sigma^0(1 + \frac{1}{\dot{w}_0}\frac{\partial^2 w}{\partial\theta^2})$, is an additional resisting moment arising from the different locations of points, z, through the shell thickness on the yield ellipse (Figure 11), which is defined by the equation:

$$\sigma_x^2 - \sigma_x\sigma_\theta + \sigma_\theta^2 = \sigma_y^2 \tag{120}$$

The strain rate vectors at the outer, mid and inner surfaces are of different magnitudes on the yield surface giving rise to a strain differential through the shell thickness and thus a resisting moment. This moment has been termed the 'directional moment' in reference [20] and is dependent on a biaxial stress state. The second term of M_θ is referred to as the 'strain hardening' moment and depends on the existence of E_h.

The equation of motion is found by substituting the curvature and force-moment expressions, equations (111) and (117) to (119) into equation (7), giving:

$$\frac{1}{a^2}\frac{\partial^2 M_\theta}{\partial\theta^2} - N_\theta[\frac{1}{a} + \frac{(w_0 + w)}{a^2} + \frac{1}{a^2}\frac{\partial^2 w}{\partial\theta^2}] + \rho h\frac{\partial^2(w_0 + w)}{\partial t^2} = 0 \tag{121}$$
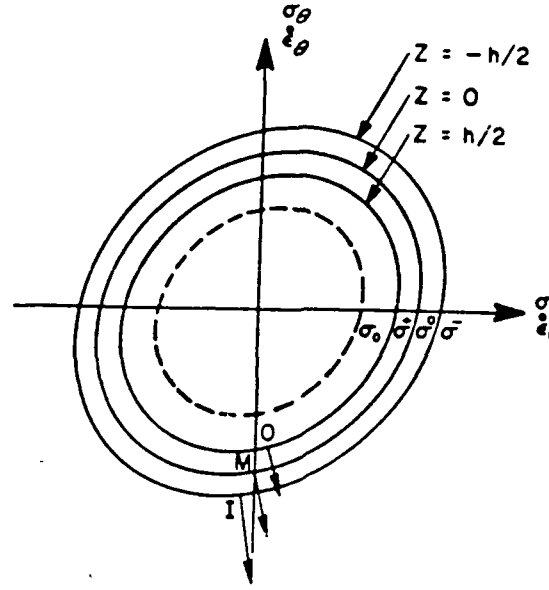
Figure 11: Strain Vectors on Yield Ellipse (from reference [20])

Simplifying assumptions are introduced by Lindberg and Vaughan [20]; the hoop thrust is made constant with time: $N_\theta = -\sigma_0 h$, the $(w_0 + w)/a^2$ term in the curvature is neglected, and the $4(w - w_i)$ term in M_θ (equation (118)) is neglected. This yields equation (121) as:

$$\frac{h^3}{36a}[\sigma^0(1 + \frac{1}{\dot{w}_0}\frac{\partial^2 w}{\partial\theta^2}) + 3\frac{E_h}{a}\frac{\partial^2(w - w_i)}{\partial\theta^2}] + \frac{\sigma_0}{a^2}\frac{\partial^2 w}{\partial\theta^2} + \rho\frac{\partial^2 w}{\partial t^2} = 0 \qquad (122)$$

where the four terms represent, respectively, the directional moment, the strain hardening moment, the hoop thrust and the inertia. With the introduction of the dimensionless parameters: $u = w/a, u_i = w_i/a, u_0 = w_0/a, \tau = V_0 t/2a, \tau_f = \rho V_0^2/2\sigma_y, \alpha^2 = h^2/12a^2$ and $\beta = E_h/\sigma_y$, equation (122) becomes:

$$\frac{\alpha^2}{c}\frac{\partial^2}{\partial\theta^2}[\frac{1}{\dot{u}_0}\frac{\partial^2 u}{\partial\theta^2} + 3\beta\frac{p^2(u - u_i)}{\partial\theta^2}] + \frac{\partial^2 u}{\partial\theta^2} + \frac{\tau_f}{2}\frac{\partial^2 u}{\partial\tau^2} = 0 \qquad (123)$$

which is similar to equation (41) of the plane strain plastic flow buckling case except that the 'directional moment' term has been added and u has been neglected with respect to 1.

The equation of motion for the unperturbed motion, equation (108), is given, from the simplifying assumptions, as $\sigma_y = -a\rho\ddot{w}_0$, which, when put in nondimensional form gives: $\ddot{u}_0 = -2/\tau_f$. Initial conditions, $w_0 = 0$ and $\dot{w}_0 = V_0$ yield $u_0 = 0$ and $\dot{u}_0 = 2$. Integration of $\ddot{u}_0$ with the initial conditions yields the dimensionless hoop velocity:

$$\dot{u}_0(\tau) = 2(1 - \tau/\tau_f) \qquad (124)$$

35

and the dimensionless hoop displacement:

$$u_0(\tau) = 2(\tau - \tau^2/2\tau_f). \tag{125}$$

The time at which motion ceases ($\dot{u}_0 = 0$), is τ_f and the midsurface hoop strain at this time is $w_0/a = u_0(\tau_f) = \tau_f$. Reference [20] introduces a further parameter, $\xi = 1 - \tau/\tau_f$, such that the period of motion is now defined in the interval $0 \leq \xi \leq 1$. The equation of motion is now expressed as:

$$\frac{\partial^2 u}{\partial \xi^2} + 2\tau_f \frac{\partial^2 u}{\partial \theta^2} - \alpha^2 \frac{\partial^2}{\partial \theta^2}[\frac{1}{3\xi}\frac{\partial^3 u}{\partial \xi \partial \theta^2} - 2\tau_f \beta \frac{\partial^2}{\partial \theta^2}(u - u_i)] = 0. \tag{126}$$

The perturbations of the fundamental motion are expressed in sine series as:

$$u(\theta, \xi) = \sum_1^\infty u_n(\xi) \sin n\theta \tag{127}$$

with initial shape:

$$u_i(\theta, 1) = \sum_1^\infty a_n \sin n\theta \tag{128}$$

and initial velocity perturbations:

$$V = V_0(1 + \sum_1^\infty b_n \sin n\theta) \tag{129}$$

yielding the Bessel type differential equation:

$$\ddot{u}_n - \frac{Q_n}{\xi}\dot{u}_n - R_n^2 u_n = S_n a_n \tag{130}$$

subject to initial conditions:

$$u_n(1) = a_n \text{ and } \dot{u}_n(1) = -2\tau_f b_n \tag{131}$$

where:

$$Q_n = \frac{\alpha^2 n^4}{3}, \quad R_n^2 = 2\tau_f n^2(1 - \alpha^2 \beta n^2), \text{ and } s_n = 2\tau_f \alpha^2 \beta n^4 \tag{132}$$

The solution of equation (130) takes the form of Bessel functions and is [20], for $R_n^2 > 0$:

$$u_n(\xi) = A_n(\xi)a_n + B_n(\xi)b_n \tag{133}$$

where:

$$
\begin{aligned}
A_n(\xi) &= 2\tau_f \xi^v[I_v(R_n\xi)K_{v-1}(R_n) + K_v(R_n\xi)I_{v-1}(R_n)](R_n + S_n/R_n) - S_n/R_n^2 \\
B_n(\xi) &= 2\tau_f \xi^v[-I_v(R_n\xi)K_v(R_n) + K_v(R_n\xi)I_v(R_n)]
\end{aligned} \tag{134}
$$

36
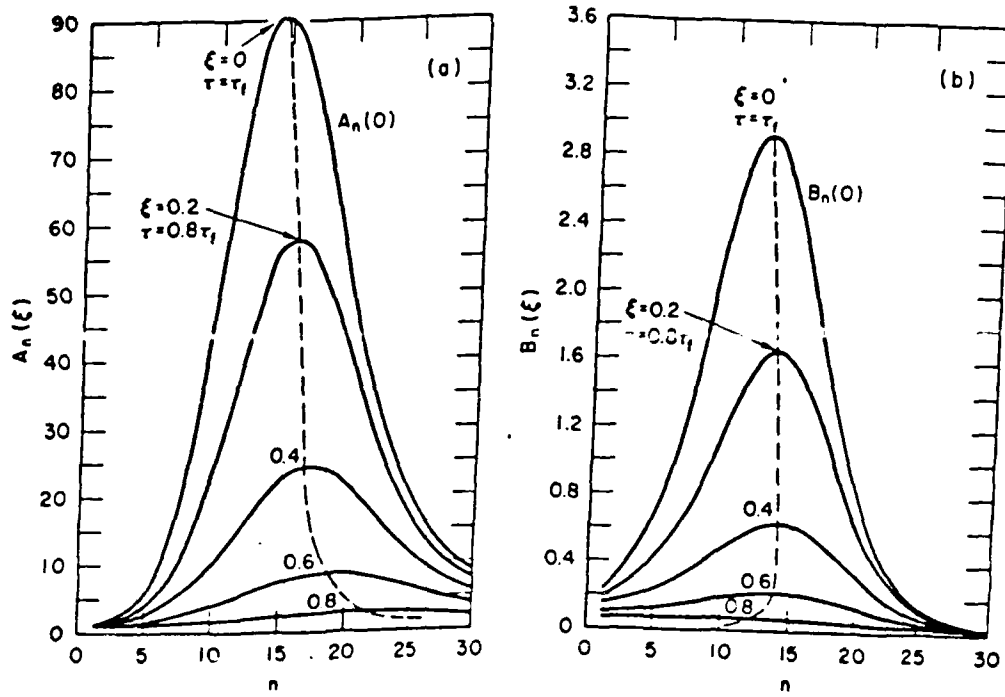
Figure 12: Displacement and Velocity Amplifications as a Function of Harmonic Number for A Short Cylinder (from reference [20])

where I_v and K_v are modified Bessel functions of the first and second kind of order $v = (\frac{1+Q_n}{2})$. The restriction $R_n^2 > 0$ defines the range of harmonics, n, which will grow unbounded, as $n^2 < 1/\alpha^2\beta$. For $R_n^2 < 0$, the solution is in terms of J_v and Y_v unmodified Bessel functions which do not become unstable. This is similar to the plane strain case where hyperbolic functions represent the unbounded range of n, and circular functions, the bounded n. The $A_n(\xi)$ and $B_n(\xi)$ functions represent amplifications of the shape and velocity imperfections, respectively. Equation (130) may also be evaluated numerically. The amplification functions $A_n(\xi)$ and $B_n(\xi)$ resulting from numerical integration, are shown in Figure 12. These are similar in form to Figures 3 and 4. The exact values of the amplified parameters are dependent on the initial shape and velocity imperfections. Although the displacement amplification functions are greater than the velocity amplifications, the two terms may be comparable for realistic initial imperfections. An approximate formula for the critical mode is given in reference [20]:

$$n_{cr} = (72)^{1/4}\sqrt{\frac{a}{h}} \tag{135}$$

Reference [21] carries the theory for short shells to shells of variable length by introducing the parameter, k, into the strain rate relation, such that:

$$\dot{\epsilon}_x = -k\dot{\epsilon}_\theta \text{ for } 0 \leq k \leq 1/2 \tag{136}$$

37

Figure 13: Yield Ellipse for Variable Length Shells (from reference [21])

where k=1/2 for the plane stress, short shell case just described, and k=0 for the infinite shell, plane strain case. Figure 13 shows the yield ellipse of the midsurface strains for varying shell length. The shaded region is entirely in a state of biaxial compression with the short shell case (k=1/2), corresponding to $\sigma_x = 0$. The stress state is expressed in terms of k as:

$$\frac{\sigma_x}{\sigma_\theta} = \frac{1-2k}{2-k} \tag{137}$$

The value of k varies along the length of the shell, being near zero at the middle of a long shell and near one half at the ends of the shell. An approximate formulae for k as a function of length is given [4], as:

$$k(x) = \frac{\cosh(2\Omega\frac{x}{D})}{2\cosh(\Omega\frac{L}{D})} \text{ for } -L/2 \le x \le L/2 \tag{138}$$

where L is the cylinder length, D is the diameter and:

$$\Omega^2 = \frac{(2-k)K_1}{[K_1 - (1-2k)^2]} \tag{139}$$

The theory for the variable length shells follows that of the short shells, but includes additional parameters as a result of:

$$\dot{\epsilon}_x = k\dot{w}_0/a \tag{140}$$

38

which are defined as:

$$K_1 = 2(1 - k + k^2), \; K_2 = \sqrt{3K_1/2}, \; \text{and,} \; K_3 = (2 - k)/K_1 \qquad (141)$$

Only the key equations, with the K_i parameters, will be repeated here . The solution of the unperturbed radial motion is defined by equation (110) which now becomes:

$$\frac{w_0}{a} = \frac{V_0}{\lambda c_h} \sin(\lambda c_h t/a) - \frac{3\sigma_y}{2K_2 E_h}[1 - \cos(\lambda c_h t/a)] \qquad (142)$$

where $\lambda^2 = \frac{2}{3}(2-k)$. This solution is reduced to that of equation (125) for a constant midsurface stress, σ_m, giving:

$$\frac{w_0}{a} = \tau(2 - \tau/\tau_f) \qquad (143)$$

with τ_f now defined as:

$$\tau_f = \frac{\rho V_0^2 K_2}{2\sigma_m(2 - k)}. \qquad (144)$$

σ_m is taken as the average stress in the post yield region as was used in section 2.1. This is different than the short shell theory which uses σ_y, which is the yield stress (ie.$\sigma_m > \sigma_y$).

The resultant moments and forces for the perturbed motion, equations (117 to 119), become:

$$M_x = \frac{h^3}{12a}[\frac{3k\sigma_m K_3}{(2 - k)K_2}(1 + \frac{1}{\dot{w}_0}\frac{\partial^2 \dot{w}}{\partial \theta^2}) - 2(2k - 1)\frac{K_3 E_h}{3a}(w_0 + \frac{\partial^2}{\partial \theta^2}(w - w_i))] \qquad (145)$$

$$M_\theta = \frac{h^3}{12a}[\frac{3k^2\sigma_m K_3}{(2 - k)K_2}(1 + \frac{1}{\dot{w}_0}\frac{\partial^2 \dot{w}}{\partial \theta^2}) + 2(2 - k)\frac{K_3 E_h}{3a}(w_0 + \frac{\partial^2}{\partial \theta^2}(w - w_i))] \qquad (146)$$

$$N_x = \frac{\sigma_m h}{K_2}(2k - 1) \; \text{and} \; N_\theta = \frac{\sigma_m h}{K_2}(-2 + k) \qquad (147)$$

where, again, M_θ consists of a 'directional moment' resulting from a strain differential on the yield surface through the shell thickness and a 'hardening moment' resulting from an E_h of positive slope creating a strain differential through the shell thickness.

The above force, moment and curvature relations are substituted into the equation of motion (equation 121), resulting in the nondimensional equation of motion:

$$\frac{\partial^2 u}{\partial \tau^2} + 2\tau_f \frac{\partial^2 u}{\partial \theta^2} - \alpha^2 \frac{\partial^2}{\partial \theta^2}[\frac{3k^2 K_3}{(2 - k)^2 \xi}\frac{\partial^3 u}{\partial t \partial \theta^2} - \frac{2(2 - k)\tau_f \beta}{K_2}(\frac{\partial^2 u}{\partial \theta^2} - \frac{\partial^2 u_i}{\partial \theta^2})] = 0 \qquad (148)$$

where the nondimensional quantities are defined in equation (123) except that σ_m replaces σ_y and τ_f is defined by equation (144). Using the same displacement perturbations (equation 127), initial distortion (equation 128), velocity imperfections (equation 129), and initial

39

conditions (equation 131), the same Bessel type differential equation as equation (130) results. The coefficients are now redefined in terms of k as:

$$Q_n = \frac{3\alpha^2 n^4 k^2 K_3}{(2-k)^2}, \quad R_n^2 = 2\tau_f n^2[1 - (2-k)\frac{\alpha^2 \beta n^2}{K_2}], \quad \text{and,} \quad S_n = 2\tau_f n^2 - R_n^2 \qquad (149)$$

with solution defined by equations (133) and (134). The amplification functions $A_n(\xi)$ and $B_n(\xi)$ behave as in Figure 12.

Both references [21] and [20] develop simplified expressions for the amplification functions by approximating their final values at $\xi \to 0$. In considering the modified Bessel functions at their limits, it can be shown that:

$$Lt_{\xi \to 0}\xi^v I_v(R_n\xi) = 0 \quad \text{and} \quad Lt_{\xi \to 0}\xi^v K_v(R_n\xi) = \frac{2^{v-1}\Gamma(v)}{R_n^v} \qquad (150)$$

where $\Gamma(v)$ is the Gamma function, and for $R_n >> v$, it can be shown that:

$$I_v(R_n) \simeq \frac{e^{R_n}}{\sqrt{2\pi R_n}} \qquad (151)$$

which result in approximations for A_n and B_n at $\xi = 0$ of:

$$A_n(0) \simeq \frac{\Gamma(v)e^{R_n}\tau_f n^2}{4(\pi)^{1/2}(R_n/2)^{v+3/2}} \quad \text{and} \quad B_n(0) \simeq \frac{\Gamma(v)e^{R_n}\tau_f}{2(\pi)^{1/2}(R_n/2)^{v+1/2}}. \qquad (152)$$

For k approaching a value of zero for the long shell, plane strain case, $Q_n = 0$, $R^2 = 2\tau_f n^2(1 - 2\frac{\alpha^2 \beta n^2}{\sqrt{3}})$, and $S_n = 4\tau_f \frac{\alpha^2 \beta n^4}{\sqrt{3}}$ and the solution of equation (130) now is in the form of hyperbolic amplification functions:

$$A_n(\xi) = (2\tau_f n^2/R_n^2)\cosh R_n(1 - \xi) - S_n/R_n^2 \qquad (153)$$

and:

$$B_n(\xi) = (2\tau_f/R_n)\sinh R_n(1 - \xi) \qquad (154)$$

which for terminal motion ($\xi = 0$), are approximated by:

$$A_n(0) \simeq \tau_f e^{R_n}n^2/R_n^2 \quad \text{and} \quad B_n(0) \simeq \tau_f e^{R_n}/R_n \qquad (155)$$

Differentiating either of equations (155), with respect to n to obtain its maximum value yields:

$$n_{cr} = \sqrt{\frac{\sqrt{3}}{4\alpha^2\beta}} \qquad (156)$$

40

with amplifications:

$$A_{n_{cr}}(0) = e^{R_n} \text{ and } B_{n_{cr}}(0) = \tau_f e^{R_n}/R_n \tag{157}$$

where $R_n = \tau_f n_{cr}^2 = \frac{\sqrt{3}\tau_f}{4\alpha^2\beta}$ and τ_f, the final circumferential strain is:

$$\tau_f = \frac{\sqrt{3}\rho V_0^2}{4\bar{\sigma}}. \tag{158}$$

For k approaching a value of 1/2 for the short shell, plane stress case, the strain hardening moment becomes negligible, giving $S_n \simeq 0$ and $R_n^2 \simeq 2\tau_f n^2$. The maximum harmonic, n_{cr}, is determined from maximizing equation (152) with respect to n. Reference [4] presents the equation for n_{cr} resulting from a graph of Q_n vs R_n as:

$$n_{cr}^3 = \frac{c\sqrt{2\tau_f}(2-k)K_1}{3k^2\alpha^2} \tag{159}$$

where; c=5/14 for A_n and c=5/17 for B_n. Approximate amplifications for the critical mode for $\alpha^2\beta n^2 \ll 1, Rn^2 \simeq 2\tau_f n^2$ and k=1/2 are given by reference [20] as:

$$\overline{A}_{n_{cr}} = \frac{e^{R_n}}{2R_n} \text{ and } \overline{B}_{n_{cr}} = \frac{\tau_f e^{R_n}}{R_n^2}. \tag{160}$$

An important conclusion from studying the effect of length in plastic flow buckling is that the number of waves (n_{cr}) in the buckled mode increases with shell length. For the same load and a/h value, a short shell with k=0.5 buckled with wave number 13, compared to its longer counterpart of k=0, which buckled with wave number 21 [21].

For the general case where both directional and strain hardening moments are significant, Lindberg and Florence [4] again derive an expression for the critical mode n_{cr}, by minimizing $A_n(\xi)$ with respect to n to obtain:

$$n_{cr}^3 = C(q)\frac{\sqrt{2\tau_f}(2-k)K_1}{3k^2\alpha^2}f(\frac{n_{cr}}{\bar{n}}) \tag{161}$$

where: $C(q) = c(c_1 e^{-q/q_0})$ and c=0.36, $c_1 = 0.85$, q_0=0.1, $q > 0.01$, $q = \frac{k^2 K_2}{2(2-k)^2 K_1 \tau_f \beta}$, $f(\frac{n_{cr}}{\bar{n}}) = \sqrt{1-(\frac{n_{cr}}{\bar{n}})^2}$ and $\bar{n}^2 = \frac{K_2}{(2-k)\alpha^2\beta}$.

The approximations to the amplification functions, $A_n(0)$, can be used to establish critical buckling velocities and impulses by establishing a limiting value of $A_n(0)$. This is done in Section 3.

41

2.4.2 Elastic Pulse Buckling of Finite Length Shells

McIvor and Lovell [23], address the topic of autoparametric, elastic response of pulse loaded finite length cylinders in the same manner as Goodier and McIvor [10] for infinite length cylinders, described in Section 2.2. Expressions for the membrane and bending energy are derived and given in Reference [23]. These are considerably more complex than those of equation (42), as the axial strain must also be considered in the energy integral. Displacement functions:

$$u(x, \theta, t) = \sum_{m=0}^{\infty} \sum_{n=0}^{\infty} U_{mn}(t) \sin \frac{m\pi x}{l} \cos n\theta$$

$$v(x, \theta, t) = \sum_{m=0}^{\infty} \sum_{n=0}^{\infty} V_{mn}(t) \cos \frac{m\pi x}{l} \sin n\theta$$

$$w(x, \theta, t) = \sum_{m=0}^{\infty} \sum_{n=0}^{\infty} W_{mn}(t) \cos \frac{m\pi x}{l} \cos n\theta \tag{162}$$

are assumed which now consider axial variation of the shell generator. Boundary conditions which facilitate a solution have been assumed; $\frac{\partial u}{\partial x}, u$, radial and circumferential shear are zero and v and w are non-zero at the ends. These boundary conditions are not neccessarily of most interest in practical problems. Expressions (162) are substituted into the energy expressions which are in turn used in the Lagrange equation, (47), to determine the equations of motion with U_{mn}, V_{mn} and W_{mn} as generalized coordinates. These expressions are similar in form to equations (48) and (49) of the infinite length case but are considerably more complex and have three pairs of equations for each of u, v and w, whereas the infinite length case only considered the radial displacement, w.

For a radial, impulsive velocity on the shell, the equation of motion (Lagrange's equation) for the fundamental hoop mode (n=m=0) is reduced to [23]:

$$\ddot{w}_{00} + w_{00} = 0 \tag{163}$$

With initial conditions $w_{00}(0) = 0$ and $\dot{w}_{00}(0) = aV_0/c$, where $c = E/\rho(1 - \nu^2) = E_l/\rho$ and the initial velocity V_0, is much less than c for elastic response, the solution to equation (163) is:

$$w_{00}(\tau) = \frac{aV_0}{c} \sin \tau \tag{164}$$

where $\tau = ct/a$. Perturbations of the higher order harmonic terms are used to investigate stability with initial velocity imperfections given by:

$$\dot{w}_{mn}(0) = \gamma_{mn} \frac{aV_0}{c} \text{ for } \gamma_{mn} \ll 1 \tag{165}$$
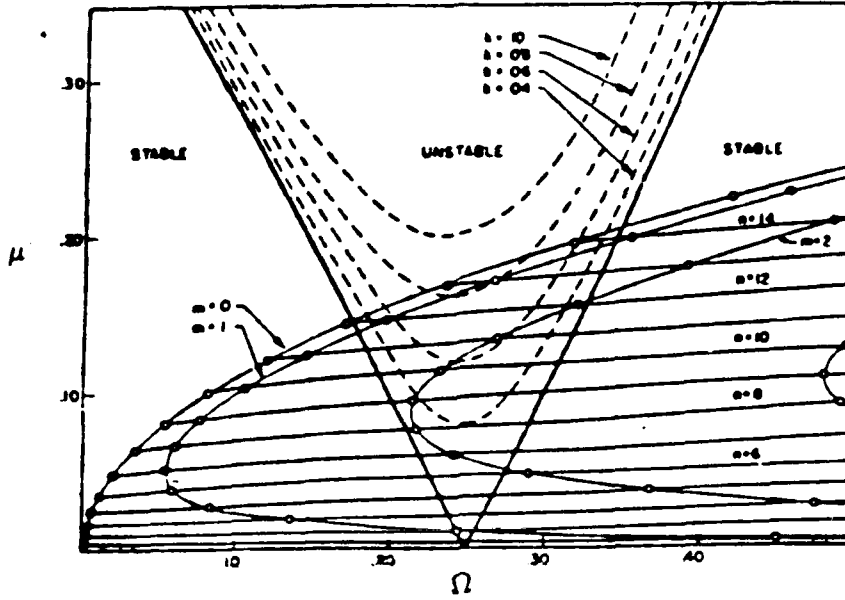
42

Figure 14: Mathieu Stability Curve for Finite Length Shell (from reference [23])

Considering products of perturbations to be negligible, the Lagrange equations for generalized displacements, U_{mn}, V_{mn} and W_{mn} become:

$$\ddot{U}_{mn} + C_1 U_{mn} + C_2 V_{mn} + C_3 W_{mn} = 0$$
$$\ddot{V}_{mn} + C_2 U_{mn} + C_4 V_{mn} + C_5 W_{mn} = 0$$
$$\ddot{W}_{mn} + C_3 U_{mn} + C_5 V_{mn} + W_{mn}(C_6 + C_4 W_{00}/a) = 0 \tag{166}$$

where C_i are defined in reference [23] and are functions of m, n, h, a and l.

Neglecting tangential inertia ($\ddot{U}_{mn} = \ddot{V}_{mn} = 0$) allows U_{mn} and V_{mn} to be expressed in terms of W_{mn}, from which the latter of equations (166) can be written in the Mathieu differential equation form:

$$\ddot{W}_{mn} + (\Omega + \mu \sin \tau) W_{mn} = 0 \tag{167}$$

where $\Omega = C_6 - \frac{C_5^2}{C_4} + \frac{(C_3 C_4 - C_2 C_5)^2}{C_4(C_2^2 - C_1 C_4)}$ and is a function of the shell parameters, m and n, and $\mu = C_4 V_0/c$. The resulting Mathieu stability curve is shown in Figure 14 for the $\Omega = 1/4$ region of stability for given initial velocity and shell parameters. Parametric points (Ω, μ) are defined by intersections of families of curves of m and n. Only the $m=0$ line was present for the infinite shell case in Figure 5. As a result of finite length allowing higher axial modes of response, there are many more points in the unstable region of the Mathieu diagram. Reference [23] demonstrates that as the shell length increases, the $m=1,2,...$ lines converge with the $m=0$ line,

43

giving the response of the infinite shell (Figure 5). The response of the shell is determined by numerically integrating the equations of motion for a few of the most amplified modes. These modes are obtained from the Mathieu stability diagram and confirmed by ensuring that the response for the chosen modes is of comparable energy to the input kinetic energy. Results of numerical integration in reference [23], show that the modes of maximum amplification are not always of the $m=0$ mode as in infinite shells.

Since this analysis is for purely elastic behaviour, elastic buckling, which grows to permanent deformation or collapse before hoop mode yield, will only occur for very thin shells. The important aspect of this theory, as in the case of the infinite shell elastic response theory is that stresses are significantly amplified by the flexural modes over the purely radial hoop mode stresses. These amplifications need to be determined from the summation of the harmonic amplitudes obtained from numerical integration of the Lagrange equations. Results reported in reference [23] indicate that amplification factors as high as four for circumferential stresses and eight for axial stresses may exist.

The case of parametric instability of elastic, finite length cylinders has been addressed by several authors for nonimpulsive loads [19,15,16]. For these cases, the Donnell shell equations have been used to derive the equations of motion for the unperturbed radial and perturbed flexural motions. Bienick, Fan and Lackman [16], derive equations of motion from Donnell equations and use the Galerkin method to obtain a solution for a system of differential equations and arrive at a Mathieu type equation. Similar results to those of McIvor and Lovell [23] are attained, where an increase in the number of parametric points in the Mathieu diagram results from decreasing the length of the shell. Yao [15], gives a good discussion of the development of the Mathieu equation from Donnell shell theory and gives several examples of its use for shells loaded radially and axially. It is, however, for very thin shells under static or periodic loading.

Anderson and Lindberg [19], use Donnell shell theory to derive the equations of motion for the shell, which will be repeated here. Using the compatability equation:

$$\Delta^4 F + Eh\left[\frac{1}{a}\frac{\partial^2 w}{\partial x^2} - \left(\frac{\partial^2 w}{\partial x \partial y}\right)^2 + \left(\frac{\partial^2 w}{\partial x^2}\right)\left(\frac{\partial^2 w}{\partial y^2}\right)\right] = 0 \tag{168}$$

and equilibrium equation:

$$D\Delta^4 w - \frac{1}{a}\frac{\partial^2 F}{\partial x^2} - \frac{\partial^2 F}{\partial y^2}\frac{\partial^2 w}{\partial x^2} + 2\frac{\partial^2 F}{\partial x \partial y}\frac{\partial^2 w}{\partial x \partial y} - \frac{\partial^2 F}{\partial x^2}\frac{\partial^2 w}{\partial y^2} - p = 0 \tag{169}$$

of Donnell shell theory [24], inertial and initial displacement imperfection terms are added, from which the equilibrium equation becomes:

$$D\Delta^4 w + N_x\frac{\partial^2}{\partial x^2}(w + w_i) + 2\frac{N_{x\theta}}{a}\frac{\partial^2}{\partial x \partial \theta}(w + w_i) + \frac{N_\theta}{a^2}\frac{\partial^2}{\partial \theta^2}(w + w_i) + \frac{N_\theta}{a} + \rho h\frac{\partial^2 w}{\partial t^2} - p = 0 \tag{170}$$

44

with N_x and $N_{x\theta}$ defined by the Airy stress function, F, and N_θ defined by the Airy stress function plus the membrane force from radial motion giving:

$$N_x = \frac{\partial^2 F}{a^2 \partial \theta^2}, \quad N_{x\theta} = -\frac{\partial^2 F}{a \partial \theta \partial x} \text{ and } N_\theta = \frac{Eh}{1 - /nu^2} \frac{w_0}{a} + \frac{\partial^2 F}{\partial x^2} \tag{171}$$

The compatability equation becomes:

$$\Delta^4 F = \frac{Eh}{a} \frac{\partial^2 w}{\partial x^2} \tag{172}$$

where the variations of w_0 with θ dissappear, as w is the radial hoop mode. The stress function, F, represents the perturbed flexual motions. Nondimensional quantities are introduced in reference [19] as:

$$u = w/a, \, u_i = w_i/a, \, \xi = x/a, \, l = L/a, \text{ and, } \tau = ct/a \tag{173}$$

and the displacement and pressures are assumed to be of series form:

$$u(\xi,\theta,\tau) = u_0(\tau) + \sum_{n=1}^{\infty} u_n(\tau) \cos n\theta \sin \pi \xi/l$$

$$u_i(\xi,\theta) = \sum_{n=1}^{\infty} \delta_n(\tau) \cos n\theta \sin \pi \xi/l$$

$$p(\xi,\theta,\tau) = \frac{Eh}{a(1-\nu^2)} [p_0(\tau) + \sum_{n=1}^{\infty} p_n(\tau) \cos n\theta \sin \pi \xi/l \tag{174}$$

where displacement and pressure distribution have been assumed to be half sine wave form (simply supported ends), and $p_n(\tau)$ are the pressure perturbations from which stability can be determined. Substituting the first of equations (174) into equation (172) yields:

$$\frac{1}{a^4}(\frac{\partial^2}{\partial \xi^2} + \frac{\partial^2}{\partial \theta^2})F = -\frac{Eh}{a} \sum_{n=1}^{\infty} \frac{\pi^2}{l^2} u_n \cos n\theta \sin \pi \xi/l \tag{175}$$

F must then be of the form:

$$F = \sum_{n=1}^{\infty} \gamma_n u_n(\tau) \cos n\theta \sin \pi \xi/l \tag{176}$$

which when substituted into equation (170) yields the equations of motion:

$$\ddot{u}_0 + u_0 = p_0$$

$$\ddot{u}_n + [\alpha^2(n^2 + \frac{\pi^2}{l^2})^2 + \frac{(1 - /nu^2)(\pi/l)^4}{[n^2 + (\pi^2/l^2)]^2} - n^2 u_0]u_n = p_n + n^2 u_0 \delta_n \tag{177}$$

which must be evaluated numerically to determine the shell motion. Equation (177) is of the Mathieu type.

45

2.5 Effect of Pulse Duration on Response

The theory of the preceeding sections has been for response to ideal, perturbed axisymmetric impulsive loads where an ideal impulse, applied over a zero time period can be represented as a Dirac Delta function. The ideal impulse was applied as an initial velocity condition since it had no time dependence. In reality, an ideal impulse is difficult to achieve, as the pulse will have some finite time duration.

A time dependent loading function must be incorporated directly into the equation of motion. This was seen in Section 2.4, where the Donnell shell equation was used to investigate stability. Anderson and Lindberg [19], investigated the effect of loading rate by considering the plastic flow equation for quasi-impulsive loads and the Donnell equation, (177), for quasi-static loading. This implies that dynamic pulse buckling occurs when the shell is in the plastic flow regime, which is true for all but very thin shells, and that static buckling occurs in the elastic regime. Reference [19] defines the impulsive loads by triangular and exponential functions, giving $I = PT/2$ for the triangular shaped pulse and $I = PT$ for the exponential shaped pulse, where T is the exponential time constant.

The plastic flow equation of motion is defined, including time varying pressure and variable material properties, as [19]:

$$\ddot{u} + \frac{\alpha^2 E_t}{E}\frac{\partial^4 u}{\partial \theta^4} + (\frac{\alpha^2 E_t}{E} + \frac{\sigma_\theta}{E})\frac{\partial^2 u}{\partial \theta^2} + \frac{\sigma_\theta}{E}(1+u) = p - \frac{\sigma_\theta}{E}(u_i + \frac{\partial^2 w_i}{\partial \theta^2}) \tag{178}$$

where the initial displacement imperfection and the displacement and pressure functions with perturbations are defined as:

$$u_i(\theta) = \sum_{n=1}^{\infty} \delta_n \cos n\theta$$

$$u(\theta, \tau) = u_0(\tau) + \sum_{n=1}^{\infty} u_n \cos n\theta$$

$$p(\theta, \tau) = p_0(\tau) + \sum_{n=1}^{\infty} p_n \cos n\theta \tag{179}$$

resulting in the equations of motion:

$$\ddot{u}_0 + \frac{\sigma_\theta}{E}(1 + u_0) = p_0$$

$$\ddot{u}_n + (n^2 - 1)[\frac{\alpha^2 E_t}{E}n^2 - \frac{\sigma_\theta}{E}]u_n = p_n + \frac{\sigma_\theta}{E}(n^2 - 1)\delta_n \tag{180}$$

with initial conditions $u_n(0) = \dot{u}_n(0) = 0$. Solutions of equation (180) are obtained by numerical integration as are the results for the elastic model from equation (177). Both equations are of Mathieu form.
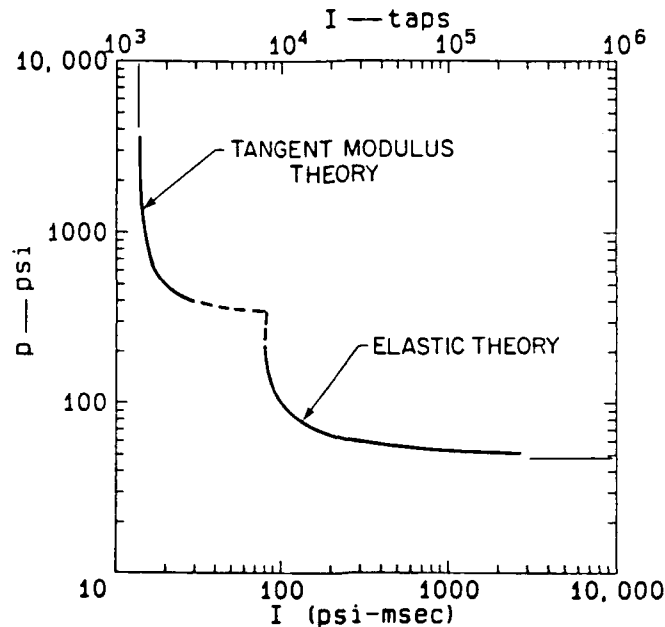
46

Figure 15: Peak Pressure versus Impulse Curves (from reference [19])

By arbitrarily assuming a critical imperfection amplification of 1000 as the buckling thresh-
old, Reference [19] derived curves from the two theories as a function of impulse versus pressure,
shown in Figure 15. The two curves are hyperbolic, approaching two asymptotes of a critical
impulse for high peak pressure and critical peak pressure for high impulse. The critical impulse
approaches the ideal impulse from the plastic flow pulse buckling theory of section 2.1 and the
critical pressure approaches the elastic, static buckling pressure for infinite time duration. The
intermediate portion of the curve, where both elastic and plastic behaviour are significant, is
not defined by either theory. Through numerical calculations it is demonstrated that for inter-
mediate a/h ratios, there are two fundamental growth modes, one of higher harmonics for the
plastic flow behaviour and one of lower harmonics for the elastic behaviour.

Lindberg and Anderson [19], investigate the effects of various parameters on the curve of
Figure 15. The pulse temporal variation, of exponential or triangular shape, showed a maximum
shift of 35 percent in the curve. Changing the a/h ratio had an expected effect of changing
the relative proportions of the two curves. For thick shells (small a/h), the hyperbolic curve of
the plastic flow theory was dominant with very little or no elastic curve in existance. For thin
shells (large a/h), the opposite behaviour occurred, with the elastic hyperbola dominating. A
change of length of the cylinder affected only the elastic branch, as the plastic flow theory used
was for infinite length cylinders.

Approximate formulae for the hyperbolic curves have been developed in reference [19], from

47
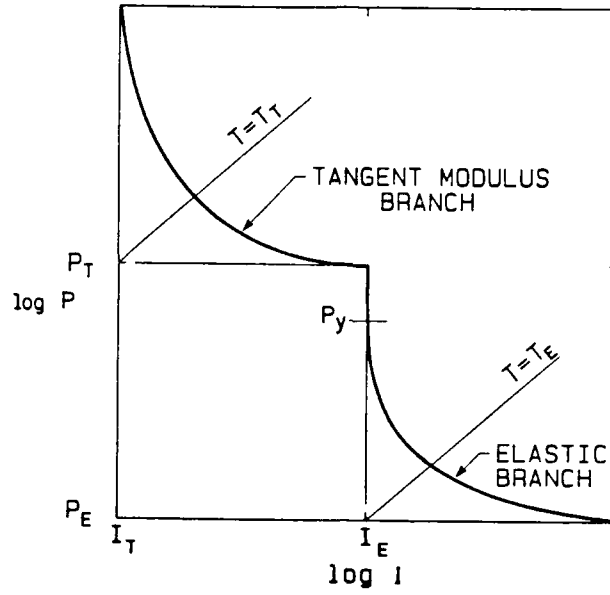
Figure 16: Peak Pressure versus Impulse Curves (from reference [19])

which, for a given shell, critical load parameters can be established. The curves are defined by:

$$[(P/P_A) - 1][(I/I_A) - 1] = 1 \tag{181}$$

where for the plastic flow curve:

$$P_A = P_T = \frac{3}{4}\sigma_y(h/a) \text{ , and,}$$
$$I_A = I_T = (96/K)^{1/4}a(\rho\sigma_y)^{1/2}(h/a)^{3/2} \tag{182}$$

and for the elastic case:

$$P_A = P_E = 0.92E(a/L)(h/a)^{5/2}$$
$$\text{and, } I_A = I_E = 5\rho ca(h/a)^2 \tag{183}$$

where K is the σ/E_t slope of the shell material. The form of curve derived from these is shown in Figure 16.

Characteristic pulse time durations are also derived, defining which theory best describes the shell behaviour:

$$T > T_T = \quad 2(a/c)\frac{\sqrt{h/a}}{\sqrt{\epsilon_y}} \quad \text{plastic flow theory}$$

$$T < T_E = \quad 5.5(L/c)\sqrt{a/h} \quad \text{elastic theory}$$

$$T_E < T < T_T \quad \text{intermediate strain reversal theory} \tag{184}$$

48

Nachbar [25] investigates the impulse to cause failure in an elastic/perfectly-plastic infinite cylinder, as a function of pressure versus time duration, for a rectangular pulse shape. Failure is assumed to occur at a specified displacement, w_f, and motion termination occurs at τ_f when $\dot{w} = 0$.

The equation of motion for the radial hoop mode is given as:

$$\rho a h \frac{\partial^2 w}{\partial t^2} = \rho R - \frac{\sigma h_0}{1 - w} \tag{185}$$

where $R = a(1 - w)$. Upon introducing nondimensional notation, equation 185 becomes :

$$\frac{\partial^2 w}{\partial \tau^2} = p(1 - u) - \frac{\sigma}{1 - w}. \tag{186}$$

After some manupulation, reference [25] presents an expression for the critical impulse under Dirac Delta function loading as:

$$I_{f_i} = \sqrt{2 \int_0^{w_f} \frac{\sigma}{1 - w} dw} \tag{187}$$

For elastic perfectly plastic material which defines $\sigma(w) = u$ for $u < u_y$ and $u = u_y$ for $u > u_y$, the critical impulse for a Dirac Delta function becomes:

$$I_{f_i} = w_y \sqrt{2 \frac{w_f}{w_y} - 1} \tag{188}$$

where $w_f < 0.1a$.

For the case where the duration of the impulse is less than the time of response spent in the elastic regime, t_y, the impulse to cause failure is given as:

$$I_f = w_y \sqrt{\Delta_f^2 + 1} \tag{189}$$

where $\Delta_f = t_f - t_y = \sqrt{2(\frac{w_f}{w_y} - 1)}$. The ratio of finite pulse to Dirac Delta function impulse is given as:

$$\frac{I_f}{I_{f_i}} = \hat{I} = \frac{T/2}{\sin T/2} \tag{190}$$

where $T \leq 2 \arccos[\Delta_f \sqrt{\Delta_f^2 + 1}]$. For the case where the pulse duration is greater than t_y,

$$\frac{I_f}{I_{f_i}} = \hat{I} = \frac{p_0}{w_y} T \sqrt{\Delta_f^2 + 1} \tag{191}$$

49
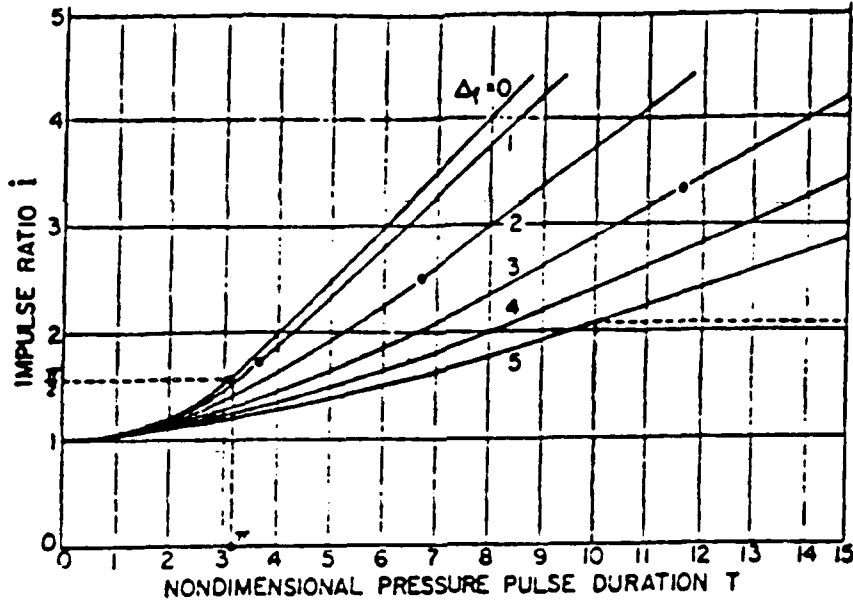
Figure 17: Critical Pulse Parameters for Axisymmetrically Loaded Cylinders (from reference [25])

where $T > 2 \arccos[\Delta_f \sqrt{\Delta_f^2 + 1}]$ and p_c is the pulse amplitude. The minimum pulse amplitude which will cause failure defined by w_f, is:

$$p_0 = w_y [\frac{1 + \Delta_f^2}{2 + \Delta_f^2}] \tag{192}$$

occuring over a pulse of duration:

$$T = T_{max} = \Delta_f \sqrt{2 + \Delta_f^2} + \frac{\pi}{2} + \arcsin \frac{1}{1 + \Delta_f^2}. \tag{193}$$

From this theory, curves of impulse ratio to pulse duration time were produced from which critical rectangular pulse parameters can be derived. These curves are shown in Figure 17 as a function of Δ_f, which is the time spent in the plastic regime.

The theory of Reference [25], has been based solely on tracking the mean radial displacement of the hoop mode, w. No flexural perturbations are considered. It is assumed that flexural buckles will form at a given ω, and that the longer the time spent in the plastic regime, the more likely it will be that flexural buckles will form.

50

2.6 Effect of Spacial Pulse Shape

In many practical problems, and certainly in the case of a submarine subject to shock loading, the pulse wave will not be axisymmetric and, in fact, will also not be applied to the entire shell instantaneously. The main restriction in assuming axisymmetry in the preceeding theory, is that the circumferential membrane stress is independent of circumferential location. In asymmetric loading functions, this is not the case. For thicker shells, which buckle in plastic flow at higher harmonics, it has been postulated [27,19,4], that if the circumferential stress can be assumed to be constant over a few buckled wave lengths, then the maximum circumferential stress, σ_θ, can be used in the axisymmetric pulse buckling equation. This requires that a finite element analysis of sufficient accuracy to predict the peak membrane stress of the shell, σ_θ, as a function of time, be undertaken. These values are then used in the numerical integration of the axisymmetric equations for perturbed motion.

In thinner shells, or for shells with longer duration pulses, the buckled wave lengths will be longer (smaller number of harmonics, n), and it is less likely that the circumferential stress will remain constant over one wavelength. This also depends, in both thick and thin shells, on the degree of asymmetry in the loading function which must be at least smoothly varying.

An impulse loading of the distribution described by:

$$I = I_c \cos\theta, \text{ for, } -\pi/2 \le \theta \le \pi/2$$
$$= 0, \text{ for, } \pi/2 < \theta < 3\pi/2 \tag{194}$$

was investigated in reference [4]. Experimental results indicated that buckling took place over about 120 degrees of the shell. Studies utilizing σ_θ results from finite element analysis, comparing peak impulse values to give the same deflection amplitude, indicate that a greater peak impulse is required for the cosine distribution. This varies from about 20 percent greater for the thick shell-plastic flow case to 100 percent greater for the thin shell-elastic case. It was also determined [4] that for the cosine pulse, the a/h ratio at which the behaviour is purely elastic is shifted much higher. For the axisymmetric pulse, a/h=288 and for the cosine pulse it increases to 480.

51

2.7 Strain Rate Reversal

In the plastic flow theory the assumption was made that the shell was in a continuous state of compression. In fact, as the buckles grow with time, the outer and inner fibers of the shell will see some reversal of strain rate, with tension zones eventually occurring in the convex parts of the buckles. The effects of strain rate reversal on the simple theory outlined in section 2.1 were investigated by Lindberg and Kennedy [26] through a numerical finite element computer code which modelled layers through the shell thickness to obtain correct strain distribution and more complete results. Two main differences from the simple theory were noted in this study.

The time to final response was shorter in the finite element code results, as the additional loss of energy from the hoop mode to the flexural mode was modelled. In the simple plastic flow theory, it was assumed that the hoop mode absorbed all of the initial kinetic energy before motion ceased. This shorter response time resulted in the simple theory overestimating the buckled amplitudes as they were allowed more time to grow.

The occurrence of strain rate reversal caused the buckles to unload elastically. This greatly increased the stiffness of the buckles as the elastic modulus instead of the strain hardening modulus was in effect. The motion of the higher harmonics was significantly curtailed as the higher harmonics have higher curvatures and thus experience strain rate reversal earlier. The result was that buckling occurred at significantly lower harmonic numbers than the simple theory predicted. Figure 18 shows the results for harmonics $n=20$ and $n=30$, comparing the finite element computer code theory to the simpler plastic flow theory. The predominant harmonic of the simple theory was $n=30$, and of the code results was $n=20$. The simpler theory significantly overexaggerated the response based on using the incorrect $n=30$ harmonic but reasonable agreement was attained for the $n=20$ harmonic between both methods.
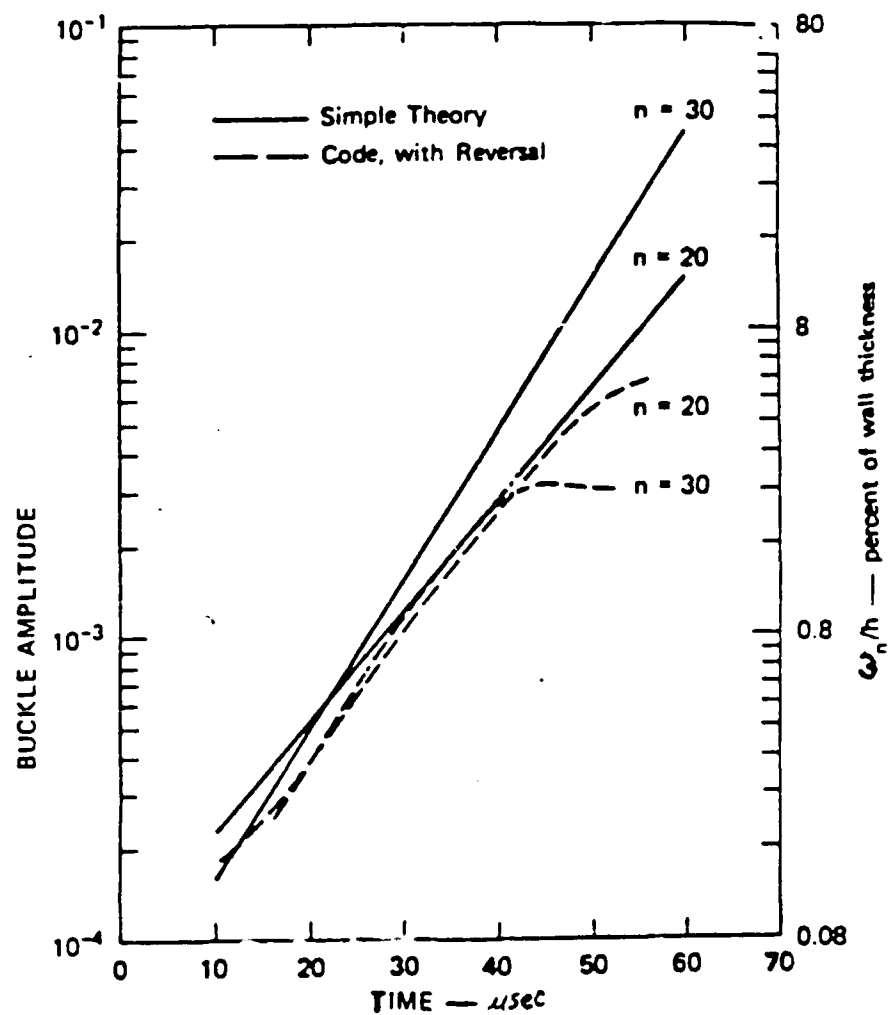
52

Figure 18: Comparison of Finite Element Results Including Strain Rate Reversal with Simpler Plastic Flow Results (from reference [4])

53

2.8 Material Property Effects

For impulsive loading, the effect of high strain rate on material properties may be significant. It is well known that the yield stress of a material may increase under high strain rates. This effect, although acknowledged, has not been specifically considered in available references for pulse buckling. Increased yield stress will affect the elastic response theory (Section2.2) if Young's Modulus is changed. The effect of increased yield stress on the plastic flow theory will be to increase the membrane flow stress value of equation(3). For more complete theory, where variable material properties are included via numerical integration of the equations of motion, a strain rate sensitive material curve could be used, if it were known.

Another strain rate effect is that of viscoelasticity and viscoplasticity, where the modulus can be very dependent on strain rate. For response to pulse loading, the strain rate continuously decreases with the motion as it comes to rest. This means that a continuously varying modulus must be considered in the analysis. Lindberg and Florence [4] have addressed pulse buckling response of finite length cylindrical shells of viscoplastic material. This follows the theory of Section 2.4 for plastic flow buckling of finite length shells. A relationship between generalized stress and generalized strain rate for viscoplastic material is used:

$$\gamma \dot{\epsilon} = \sigma / \sigma_0 - 1 \tag{195}$$

where γ is the viscosity constant from material tests and σ_0 is the generalized stress at infinitesimally small strain rate. The equation of motion for the unperturbed radial motion is:

$$\ddot{w}_0 + \frac{2(2-k)}{3a^2\rho}\sigma_0\lambda\dot{w}_0 = \frac{-(2-k)\sigma_0}{K_2 a\rho} \tag{196}$$

which varies from the plastic case by the term $\sigma_0\lambda\dot{w}_0$ replacing $E_h w_0$. The solution of equation (196) is given as:

$$w_0 = [V_0 + \frac{3a}{2\gamma K_2}][1 - e^{-2(2-k)\frac{\sigma_0\gamma t}{3a^2\rho}}]\frac{3a^2\rho}{2(2-k)\sigma_0\gamma} - \frac{3at}{2\gamma K_2}. \tag{197}$$

The equation of motion for the perturbed flexural motions, is given, in the nondimensional parameters used in equation (148), as:

$$\ddot{u} - \frac{\alpha^2}{(2-k)}(\frac{3k^2}{K_1\xi} + \frac{4\gamma V_0}{3a})\frac{\partial^4 u}{\partial\theta^4} + 2\tau_f\frac{\partial^2 u}{\partial\theta^2} = 0 \tag{198}$$

in which the second term varies from the non-viscoplastic case of equation (148). By making the substitutions of equations (127) to (130), the governing equation becomes:

$$\ddot{u}_n - (P_n + Q_n/\xi)\dot{u}_n - R_n^2 u_n = 0 \tag{199}$$

54

where: $P_n = \frac{4\alpha^2 \gamma V_0 K_2 n^4}{3(2-k)a}$ and $Q_n = \frac{3\alpha^2 k^2 n^4}{(2-k)K_1}$, with solution in the same form as the non-viscoplastic case:

$$u_n(\xi) = A_n(\xi)a_n + B_n(\xi)b_n \tag{200}$$

where $A_n(\xi)$ and $B_n(\xi)$ are the amplification functions for the displacement and velocity perturbations and are now defined in terms of Kummer functions and given in reference [4, pg 246].

Experimental work reported in Reference [4] demonstrated that for fully annealed 1015 steel, the effects of increased strain rate were increased the yield stress and lengthened plastic portion of the material curve. A relationship for increase in yield stress with strain rate is postulated by Symonds and Bodner[28] as:

$$\sigma/\sigma_y = 1 + (\dot{\epsilon}/D)^{1/p} \tag{201}$$

where σ_y is the static yield stress and p and D are constants dependent on the material (5 and 40.4 respectively, for mild steel).

The key material parameter in plastic flow buckling is the tangent modulus. If the tangent modulus is assumed to be constant (linear plastic regime), closed form solutions are attainable. The tangent modulus is not usually linear, in which case numerical integration of the equations of motion is required. A description of the material curve used in much of the work is:

$$\begin{aligned}
\frac{\sigma}{E_t} \quad &= \sigma/E = \epsilon, \text{ for, } 0 \leq \epsilon \leq \epsilon_y \\
&= \epsilon_y + K'(\epsilon - \epsilon_y), \text{ for, } \epsilon \geq \epsilon_y
\end{aligned} \tag{202}$$

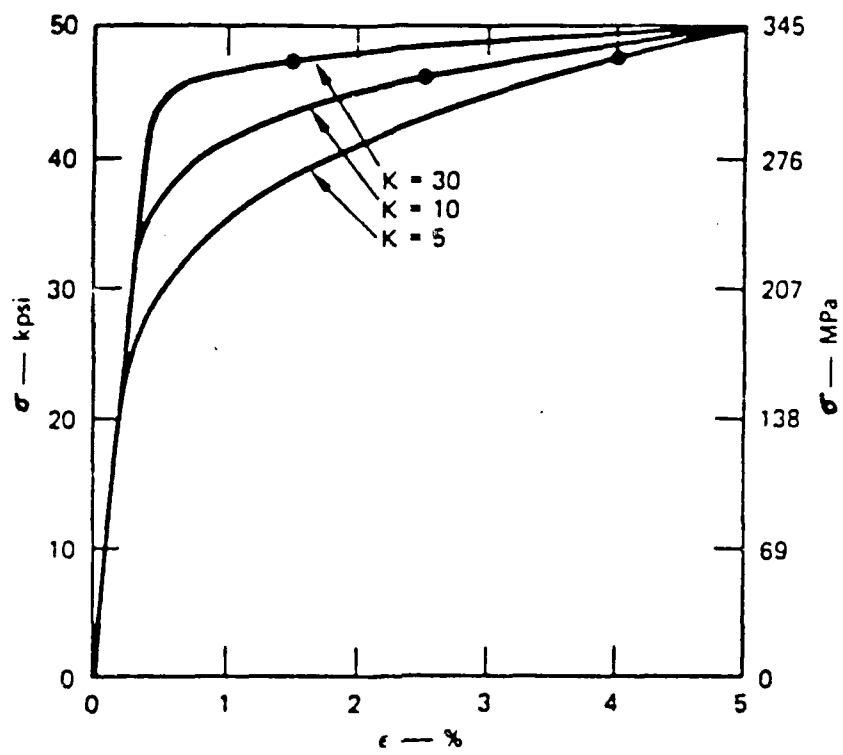which describes curves of the form shown in Figure 19.

Figure 19: Material Property Curve (from reference [4])

3 Approximate Formulae for Critical Impulse and Critical Modes of Dynamic Pulse Buckling

From the preceeding theory, formulae for the critical mode of response and for approximation of the critical impulse to produce pulse buckling have been derived.

The critical mode number (predominant harmonic of response) for plastic flow buckling of infinite cylinders or rings is given as (equation 24) [9]:

$$n_{cr}^2 = \frac{1}{2}(s^2 + 1) \tag{203}$$

which, if 1 is neglected with respect to s^2, becomes: $n_{cr} = \sqrt{6}\frac{a}{h}\sqrt{\frac{\sigma_m}{E_h}}$. Stuiver [11] derives a critical mode equation for the same case using the combined elastic-plastic theory (equation 92):

$$n_{pl} = 0.85\sqrt{6}\frac{a}{h}(\frac{\sigma_y}{E_h})^{1/2}[1 + (\beta\frac{V_0/c}{\epsilon_y})^2]^{1/4} \tag{204}$$

which gives comparable values to equation (203). For plastic flow buckling of short shells where directional moments dominate the strain hardening moments, Vaughan and Florence [20] give the critical mode (equation 135), as:

$$n_{cr} = (72)^{1/4}\sqrt{\frac{a}{h}} \tag{205}$$

For variable length shells, Lindberg and Florence [4] give the expression (equation (161)):

$$n_{cr}^3 = C(q)\frac{\sqrt{2\tau_f}(2-k)K_1}{3k^2\alpha^2}f(\frac{n_{cr}}{n}) \tag{206}$$

where the parameters are defined in section 2.4.

For viscoplastic material response, where the viscoplastic moments dominate the directional moment, reference [4] gives the critical mode as:

$$n_{cr}^3 = (\frac{3a}{8\gamma\alpha^2})\sqrt{\frac{(2-k)p}{K_2\bar{\sigma}}} \tag{207}$$

where the parameters are defined in section 2.8. All of the above formulae are for thick shells where the response is considered to be entirely plastic.

For response where behaviour is entirely elastic, equation (54) gives the critical mode for response without permanent buckling as [10]:

$$n_{cr} = 1.316\sqrt{\frac{a}{h}} \tag{208}$$

57

For larger initial impulses where buckling can occur, the empirical relation (equation (65)) gives:

$$n_{cr}^4 = \frac{0.25}{\alpha^2} + \frac{0.13V^2}{c^2\alpha^2} \qquad (209)$$

Stuiver [11], gives a value for the elastic critical mode as:

$$n_{cr} = 2\frac{a}{h}\sqrt{\frac{V_0}{c}}. \qquad (210)$$

To establish the critical impulse which will cause dynamic buckling, a limit of displacement amplitude to define the point of buckling must be defined. With simplifying assumptions on material properties and critical mode numbers. equations for approximate critical impulse have been derived.

For plastic flow buckling of infinite cylinders or rings, Lindberg and Florence [4] derive an expression for the impulse required to give a 20 fold increase in initial shape imperfection as:

$$I_{cr} = \sqrt{3}\rho c a\sqrt{\frac{E_h}{E}}(\frac{h}{a})^2 \qquad (211)$$

Lindberg and Florence also give threshold impulse values for variable length shells failing by plastic flow buckling, by taking the limit as a shape amplification of 100, ie. $A_n = 100$. For long shells, with k=0, this gives:

$$I_{cr} = 3.07\sqrt{\rho E_h}a(\frac{h}{a})^2 \qquad (212)$$

and for short shells with k=1/2, this gives:

$$I_{cr} = 2.46\sqrt{\rho\sigma_m}a(\frac{h}{a})^{3/2} \qquad (213)$$

for $q > 0.5$ where $q = \frac{3k^2K_2}{2(2-k)K_1\tau_j\beta}$. For variable length shells, the impulse functions:

$$\begin{aligned}
I &= (\frac{k^2K_3}{4K_2^2C_0^3C})^{1/4}f(\frac{N}{n}\sqrt{\rho\overline{\sigma}}a(\frac{h}{a})^{3/2}(\ln\sqrt{2e}A_n)^{3/4} \quad \text{for } 0.01 < q \\
&= (\frac{2-k}{2\sqrt{3}K_2})f_{\frac{N}{n}}\sqrt{\rho E_h}a(\frac{h}{a})^2\ln A_n \qquad \text{for } 0.01 > q
\end{aligned} \qquad (214)$$

can be used, by setting the amplification, A_n, equal to 100, and where the variables are defined in Section 2.4. For viscoplastic material response, Lindberg and Florence give the impulse amplification relation:

$$I = \frac{4}{3}[\frac{2(2-k)}{9K_2}]^{1/3}(\overline{\tau}^2h^2\rho\gamma)^{1/v}(\frac{h}{a}\ln(\frac{8A_n}{5}) \qquad (215)$$

58

for which A_n may be taken as 100 to determine critical impulses.

For buckling in the elastic regime, where the flexural buckles exceed yield before the hoop mode, a value of p=4 is used in equation (71) to give an amplification of initial shape imperfection of 65. From the relation for impulse to velocity of $I = \rho h V_0$, the critical impulse for a condition of p=4 is given [4] as:

$$I_{cr} = 1.15 \rho ca (\frac{h}{a})^2 \tag{216}$$

where the condition, $a/h \leq 1.15/\epsilon_y$, must be met to ensure the hoop motion does not exceed yield.

The curves presented in Section 2.5 from reference [19] can also be used to establish critical impulses, particularly if the loading is not for an ideal impulse.

To cover the full range of a/h values, Lindberg and Florence [4] suggest using the plastic flow and elastic buckling threshold equations, and then using whichever gives the lowest value. When these are plotted on a graph of a/h versus I_{cr}, Figure 20 results (for the given aluminum shell). The two equations defining the two buckling lines are given as:

$$\frac{I}{\rho ca} = 1.807D(h/a)^{3/2} \text{ for } a/h \leq .405/D^2$$

$$= 1.15(h/a)^2 \text{ for } a/h \geq .405/D^2 \tag{217}$$

The results of these various formulae have been investigated via a computer program for shells of various dimensions and properties. Table 2 gives the shell parameters and Table 3 gives the results.

Models 1 to 19 were used to investigate shells with increasing a/h ratios. Columns A, B and C give the critical mode from infinite cylinder, plastic flow theory. The critical mode increases with a/h and the theory becomes inapplicable for a/h much greater than 40, where elastic behaviour starts to have some influence. Columns D and E give the critical modes for the short cylinder, plastic flow theory. The greater resistance to bending resulting from the directional moment contribution is evident in the lower mode numbers for these cases. Columns F, G and H give the critical impulse and velocity to cause plastic flow buckling. As the shell becomes thinner (larger a/h), the required impulse becomes less, as would be expected. Column I gives the critical mode for the low velocity, elastic vibration response. Columns J and K give the critical modes for the larger velocity, elastic buckling case. The critical modes also increase with a/h ratio. Column L gives the critical impulse and velocity to cause elastic, dynamic pulse buckling and as in the plastic flow case, as a/h increases, the required impulse decreases.

The effect of changing the material yield stress, σ_y, is investigated with Models 3, 20 and 21. There is no change for any of the formulae except for column B which shows a decrease in the critical mode number with decreasing yield stress. This is from the elastic-plastic theory of Stuiver [11] who included some elastic effect in the determination of the plastic flow buckling
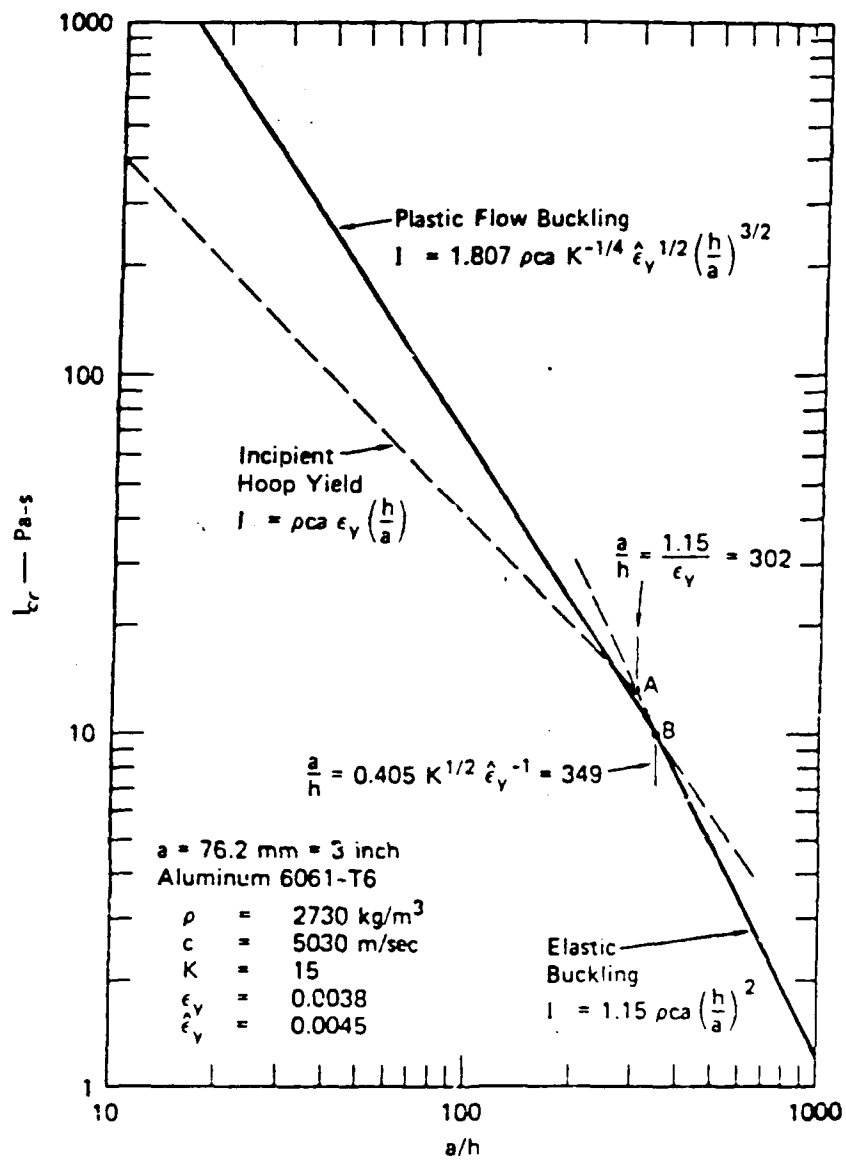
59

Figure 20: Critical Impulse Versus a/h Ratio (from reference [4])

60

critical modes. Formulae for column A and C would also be affected as they are a function of the flow stress, σ_m, which is a function of the yield stress. This can be seen in models 31 to 33 where σ_m is varied.

Models 3 and 22 to 25 were used to investigate the effect of varying the tangent modulus in the strain hardening portion of the material curve. Columns A, B and C for the infinite shell, plastic flow theory show a dramatic decrease in the critical mode for increasing tangent modulus. Columns F and G show that the required critical impulse increases with tangent modulus for the infinite shell, plastic flow case, as would be expected due to an increase in the shell stiffness. Columns D and E for the critical mode and column H for the critical impulse show no change with varying tangent modulus as these values are for the short shell case where the directional moment is assumed to be dominant over the strain hardening moment.

The effect of varying the initial velocity was investigated with Models 3 and 26 to 30. There is a slight variation in column B with the critical mode number increasing with increasing initial velocity. This is from equation (204) which shows a variation of n_{cr} as the square root of V_0. Column E shows a strong dependency of n_{cr} on V_0. The other plastic flow formulae show no variation with initial velocity. The critical impulse and velocity formulae, are, of course, not affected by V_0. The elastic critical modes for velocities large enough to cause buckling are influenced by the initial velocity. Columns J and K show that the critical mode number varies proportionally to the initial velocity.

Models 3 and 31 to 33 were used to investigate the effect of varying the flow stress value, σ_m. Columns A and C show a decrease in critical mode with decreasing flow stress. Column B, from equation (204), shows no change in critical mode with flow stress, but, the flow stress is an average value which is dependent on the yield stress and tangent modulus, which are parameters in equation (204) so some effect should be realized. This is also the case in the critical impulse formulae of columns F and G where the tangent modulus is used. The flow stress does not have any influence on the elastic theory.

61

Model	a(in)	h(in)	σ_y(psi)	σ_m(psi)	E_h(psi)	V_0(in/sec)	ρ(lb-sec^2/in^4)
1	10	1	60,000	70,000	1,000,000	6,000	0.000787
2	20	1	60,000	70,000	1,000,000	6,000	0.000787
3	30	1	60,000	70,000	1,000,000	6,000	0.000787
4	40	1	60,000	70,000	1,000,000	6,000	0.000787
5	50	1	60,000	70,000	1,000,000	6,000	0.000787
6	60	1	60,000	70,000	1,000,000	6,000	0.000787
7	70	1	60,000	70,000	1,000,000	6,000	0.000787
8	80	1	60,000	70,000	1,000,000	6,000	0.000787
9	90	1	60,000	70,000	1,000,000	6,000	0.000787
10	100	1	60,000	70,000	1,000,000	6,000	0.000787
11	120	1	60,000	70,000	1,000,000	6,000	0.000787
12	140	1	60,000	70,000	1,000,000	6,000	0.000787
13	160	1	60,000	70,000	1,000,000	6,000	0.000787
14	180	1	60,000	70,000	1,000,000	6,000	0.000787
15	200	1	60,000	70,000	1,000,000	6,000	0.000787
16	250	1	60,000	70,000	1,000,000	6,000	0.000787
17	300	1	60,000	70,000	1,000,000	6,000	0.000787
18	350	1	60,000	70,000	1,000,000	6,000	0.000787
19	400	1	60,000	70,000	1,000,000	6,000	0.000787
20	30	1	50,000	70,000	1,000,000	6,000	0.000787
21	30	1	40,000	70,000	1,000,000	6,000	0.000787
22	30	1	60,000	70,000	2,000,000	6,000	0.000787
23	30	1	60,000	70,000	3,000,000	6,000	0.000787
24	30	1	60,000	70,000	4,000,000	6,000	0.000787
25	30	1	60,000	70,000	10,000	6,000	0.000787
26	30	1	60,000	70,000	1,000,000	9,000	0.000787
27	30	1	60,000	70,000	1,000,000	5,000	0.000787
28	30	1	60,000	70,000	1,000,000	3,000	0.000787
29	30	1	60,000	70,000	1,000,000	1,000	0.000787
30	30	1	60,000	70,000	1,000,000	500	0.000787
31	30	1	60,000	65,000	1,000,000	6,000	0.000787
32	30	1	60,000	61,000	1,000,000	6,000	0.000787
33	30	1	60,000	60,000	1,000,000	6,000	0.000787

Table 2: Shell Parameters Used in Table 3

Model #	Plastic Flow Theory								Elastic Theory			
	N_{cr}					$I_{cr}-V_{cr}$ (in/s)			N_{cr}			$I_{cr}-V_{cr}$
	A	B	C	D	E	F	G	H	I	J	K	L
1	6	5	6	9	8	5.1-6465	8.6-10943	5.8-7336	4	4	3	18.5-23537
2	12	10	12	13	14	2.5-3232	4.3-5471	4.1-5187	5	7	6	9.3-11768
3	19	16	18	15	18	1.7-2155	2.9-3648	3.3-4236	7	11	10	6.2-7846
4	25	21	24	18	22	1.3-1616	2.2-2736	2.9-3668	8	14	13	4.6-5884
5	32	26	30	20	25	1.0-1293	1.7-2189	2.6-3281	9	18	17	3.7-4707
6	38	32	36	22	29	.8-1077	1.4-1824	2.4-2995	10	21	20	3.1-3923
7	45	37	42	24	32	.7-923	1.2-1563	2.2-2773	11	25	23	2.6-3362
8	51	43	48	26	35	.6-808	1.1-1368	2.0-2594	11	28	27	2.3-2942
9	58	48	54	27	38	.55-718	1.0-1216	1.9-2445	12	32	30	2.1-2615
10	64	53	60	29	40	.5-647	.86-1094	1.8-2320	13	35	34	1.9-2353
11	77	64	72	31	46	.4-539	.7-912	1.7-2118	14	42	41	1.5-1961
12	90	75	84	34	50	.36-462	.6-782	1.5-1961	15	49	47	1.3-1681
13	103	86	96	36	55	.32-404	.54-684	1.4-1834	16	57	54	1.2-1471
14	116	96	108	39	60	.28-359	.48-608	1.4-1729	17	64	61	1.0-1307
15	129	107	120	41	64	.25-323	.43-547	1.3-1640	18	71	68	.93-1177
16	162	134	150	46	74	.2,-259	.34-438	1.2-1467	20	89	85	.74-942
17	194	161	180	50	84	.17-216	.29-365	1.1-1340	22	106	102	.62-785
18	226	188	211	54	93	.15-185	.25-313	.98-1240	24	124	119	.53-673
19	259	215	241	58	101	.13-162	.22-274	.91-1160	26	142	136	.46-588
20	19	15	18	15	18	1.7-2155	2.9-3648	3.3-4236	7	11	10	5.2-7846
21	19	13	18	15	18	1.7-2155	2.9-3648	3.3-4236	7	11	10	6.2-7846
22	13	12	12	15	18	2.4-3048	4.1-5159	3.3-4236	7	11	10	6.2-7846
23	11	11	10	15	18	2.9-3721	5.5-6318	3.3-4236	7	11	10	6.2-7846
24	9	11	9	15	18	3.4-4301	5.7-7296	3.3-4236	7	11	10	6.2-7846
25	194	152	180	15	18	.17-216	.29-365	3.3-4236	7	11	10	6.2-7846
26	19	17	18	15	21	1.7-2155	2.9-3648	3.3-4236	7	13	12	6.2-7846
27	19	15	18	15	17	1.7-2155	2.9-3648	3.3-4236	7	10	9	6.2-7846
28	19	15	18	15	14	1.7-2155	2.9-3648	3.3-4236	7	8	7	6.2-7846
29	19	15	18	15	10	1.7-2155	2.9-3648	3.3-4236	7	7	4	6.2-7846
30	19	15	18	15	8	1.7-2155	2.9-3648	3.3-4236	7	7	2	6.2-7846
31	18	16	17	15	18	1.7-2155	2.9-3648	3.2-4082	7	11	10	6.2-7846
32	18	16	16	15	18	1.7-2155	2.9-3648	3.1-3954	7	11	10	6.2-7846
33	18	16	16	15	18	1.7-2155	2.9-3648	3.08-3921	7	11	10	6.2-7846

A= Eqn 203, Ref 9   E= Eqn 206, K=1/2, Ref 4   I= Eqn 208, Ref 10
B= Eqn 204, Ref 11   F= Eqn 211, Ref 4   J= Eqn 209, Ref 4
C= Eqn 206, K=0, Ref 4   G= Eqn 212, K=0, Ref 4   K= Eqn 210, Ref 11
D= Eqn 205, Ref 20   H= Eqn 213, K=1/2, Ref 4   L= Eqn 216, Ref 4

Table 3: Results of Various Formulae for Critical Modes and Impulses

4 Review of Numerical Solutions to Dynamic Pulse Buckling

Finite difference and finite element numerical methods have been used to solve a wide variety of complex structural mechanics problems, particularly where analytical solutions cannot be easily found. The successful utilization of numerical methods hinges on being able to formulate a discretized model and solution scheme capable of modelling the correct physical behaviour. For dynamic pulse buckling, this means that the model must be capable of reproducing the nonlinear, elasto-plastic motion of the shell wall in the higher harmonic modes which occur in pulse buckling.

Most numerical studies of pulse loading consider only unperturbed dynamic response and do not consider the growth of buckling modes in the solution. Element grid discretization, nonlinear formulations, solution methods, material property representation and the failure cutoff criteria are parameters which need to be investigated for numerical determination of dynamic buckling.

Ishizaki and Bathe [29], investigated static and dynamic, linear and nonlinear response of perfect and imperfect shells with the finite element program ADINA [30]. A spherical cap, a cylinder and a sphere were investigated to determine the collapse loads. For large displacement, elasto-plastic (E.P.) response, updated and total Langrangian (T.L.) kinematic formulations were investigated as well as the modified Newton and the BFGS (Broyden-Fletcher-Goldfarb-Shanno) iterative solution schemes for equilibrium [31]. Without modelling imperfection perturbations in the shell geometry, the elastic bifurcation and the elasto-plastic yield collapse loads can be determined. Figure 21a demonstrates the response of a complete sphere to a static loading. Figure 21b shows the response of the perfect sphere to a dynamic step loading of half the elastic buckling load magnitude. The elasto-plastic curve assumes a permanent set about which the response oscillates and the elastic response oscillates with greater amplitude but reaches zero displacement on each oscillation. Figure 21c shows the response to static loading of an imperfect shell. The lower curves include the geometric nonlinear total Langrangian formulation which allows the growth of the imperfections to produce instability. Figure 21d shows the response of the imperfect shell to the dynamic step load. The top curve shows the results of the elasto-plastic, total Langrangian formulation which models the unbounded growth of the imperfection. This latter curve models the physical characteristics that the analytical solutions did, that is, allowing unbounded nonlinear growth of displacements for a specified load. Two important factors in reproducing this behaviour with the finite element method are that imperfections in the modes of response must be modelled to produce the unbounded growth, and that the load amplitude has to be increased in consecutive analyses until instability occurs. Instability was established in the ADINA study at the point where the determinant of the stiffness matrix became negative (singular). Some major difficulties in formulating a solution to pulse buckling response of shells with the finite element method are evident.

The analytical solutions discussed in Section 2 indicate that the circumferential modes of predominant response (buckling growth) occur in higher harmonics than static buckling
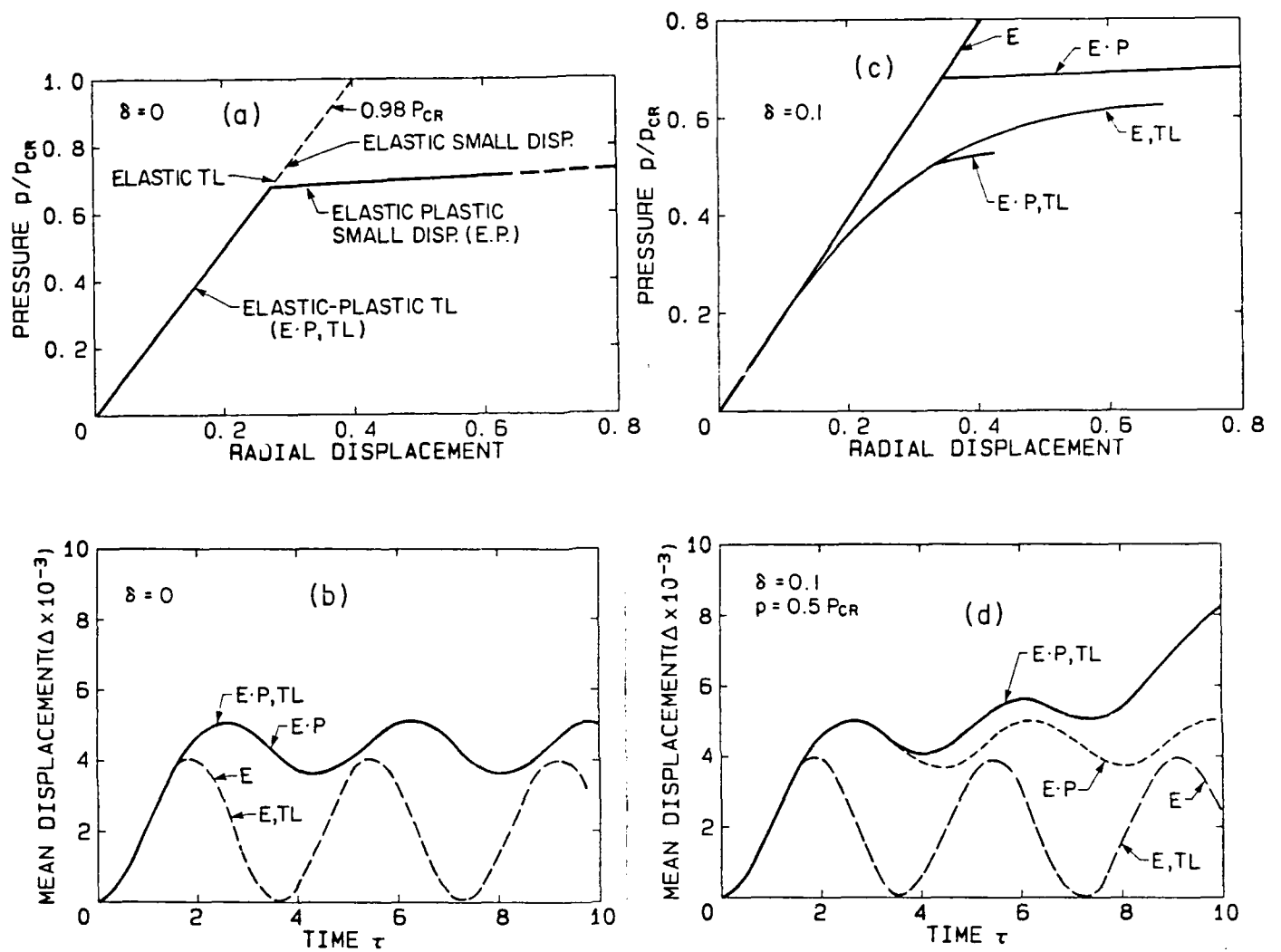
64

Figure 21: Static and Dynamic Response of a Perfect and Imperfect Sphere (from reference [29])

65

modes. It can also not be easily determined which mode will predominate. Therefore it is necessary to model imperfections for several harmonics of numbers up to 30 or higher. This requires a very high level of discretization in the circumferential direction of the shell. In determining the response of the cylindrical shell to a cosine pulse (the same problem as addressed by Lindberg and Kennedy [26]), the model was discretized with 60, 8 noded elements in one half of the circumference. Models to investigate dynamic pulse buckling, particularly as length and complexities such as stiffeners are included, will very quickly attain a large number of degrees of freedom. To determine the limit load of dynamic pulse buckling, several analyses runs at increasing load levels will be required. Thus determination of dynamic pulse buckling response by the finite element method will be an expensive and time consuming proposition. Quoting from reference [29], 'nonlinear dynamic buckling analysis is frequently beyond the current state of the art'.

Lindberg and Kennedy [26], investigate plastic flow buckling theory with a finite element code, SABOR/DRASTIC 6 [32]. This is an uncoupled, axisymmetric finite element analysis where response is investigated one mode at a time. The results of this work in relation to the plastic flow theory were discussed in Section 2.7. The formulation of the finite element problem involved modelling harmonic imperfections of the applied impulse. In this case, harmonics derived from the plastic flow theory and from experimental results were used. Good agreement between the numerical results and experiment was attained, due in part to the fact that the imperfections used in the numerical analysis were derived from the experimental results.

Wesenberg [18] investigates dynamic buckling response for shells with several a/h ratios and compares them to experimental results. These are discussed in Section 2.3. Here again, imperfection modes and amplitudes were measured from experimental results and used in the numerical finite difference formulation.

More recently (1987-88), Gefken, Kirkpatrick and Holmes [33,34,35] applied three dimensional nonlinear finite element solutions to rings and finite length thin shells with good correlation to experimental results. The necessary requirements of using a finite element solution in terms of initial imperfect shape and the level of discretization were investigated in these studies. It was determined [35] that initial imperfections expressed in the exponential form:

$$A_n = .05h \quad n \leq 10$$
$$A_n = \frac{h}{n^{1.3}} \quad n > 10 \tag{218}$$

gave the best comparison to results of models with imperfections derived from measuring actual cylinder imperfections. The finite element models were generated with a series of imperfections covering a range of harmonics such that the geometry was formed by the harmonic summation:

$$R(\theta) = R + \sum_{n=2}^{100} A_n \cos(n\theta + \phi_n) \tag{219}$$

66

Kirkpatrick and Holmes[34] used the DYNA3D finite element code with the Hughes-Lui shell element. They reported requiring approximately ten of these single-integration-point elements per buckling wavelength.

Many studies investigate the dynamic response of shell structures to impulsive loading, but do not investigate the possibility of dynamic buckling. Wu and Witmer [36] develop a layered finite element model of a curved beam including strain hardening and strain rate effects. Comparisons to experimental results from impulse loading are made. Lee and Horng [2,37] develop finite difference solutions to elasto-plastic dynamic response of ring stiffened cylinders to shock wave type loading. The critical yield points occur at the stiffener shell connection. Buckling could have been investigated if the harmonic imperfections were included in the study.

Several studies [38,39] investigate the finite element solution for displacements of cylindrical shells subject to underwater shock loads. The nonlinear loading function of the coupled fluid-structure interface is modelled using doubly asymptotic approximation and boundary elements. To investigate dynamic stability for this case, a nonlinear finite element code and modelling to include imperfections in the initial shape and pressure pulse must be used in conjunction with the loading algorithm.

5 Conclusions

Analytical solutions for specific cases of dynamic pulse buckling have been established by various authors through investigation of the growth of perturbations to the fundamental motion. Cylinders loaded with an axisymmetric pulse which respond either entirely in the elastic or entirely in the plastic material range have been investigated analytically. Approximate formulae to establish the critical modes of buckling and the critical impulses to cause buckling for various simple cases have been derived. These approximate formulae have been investigated for various shell parameters within the context of this review. The dynamic buckling response is a function of the shell dimensions, material properties and loading function. No analytical solution has been derived for dynamic buckling of shells of intermediate a/h ratios which encompass many practical cases.

For complex shell geometries, complex loading functions or shells of intermediate a/h ratios, numerical finite element or finite difference methods offer a potential solution. This is not straight forward and few studies have investigated dynamic buckling solutions using numerical methods. Material and geometric nonlinearities have to be included in the formulation and, as in the analytical solutions for the simple cases, solution is for excessive growth of initial imperfections. No studies of ring-stiffened shells were found for this literature review. A finite element solution seems to be most attractive for studying dynamic pulse buckling of submarine structure. Pressure hulls tend to be of an intermediate a/h ratio where elasto-plastic behaviour and strain rate reversal are important to the response.

The physical concepts of dynamic pulse buckling have been established through review of the analytical studies. These and the approximate formulae for critical modes and loads will be invaluable in attempting to formulate numerical solutions of more complex problems such as pulse buckling of ring stiffened submarine pressure hulls.

APPENDIX A: Derivation of the Shell Curvature Expression

The change in curvature, κ, is defined as the difference between the deformed shell curvature, $\frac{1}{\rho}$, and the initial shell curvature, $\frac{1}{a}$:

$$\kappa = \frac{1}{\rho} - \frac{1}{a}$$

The initial length of element mn, from Figure A.1, is $ds = a d\phi$, and the initial curvature is $\frac{\partial \phi}{\partial s} = \frac{1}{a}$. The length after deformation, $m_1 n_1$, is $ds + \Delta ds$, and the angle of curvature is $d\phi + \Delta d\phi$, which gives the curvature after deformation as:

$$\frac{1}{\rho} = \frac{d\phi + \Delta d\phi}{ds + \Delta ds}$$

The angle $\Delta d\phi$ is:

$$\Delta d\phi = d\phi_{n_1} - d\phi_{m_1} = \frac{\partial w}{\partial s} + \frac{\partial^2 w}{\partial s^2} ds - \frac{\partial w}{\partial s} = \frac{\partial^2 w}{\partial s^2} ds$$
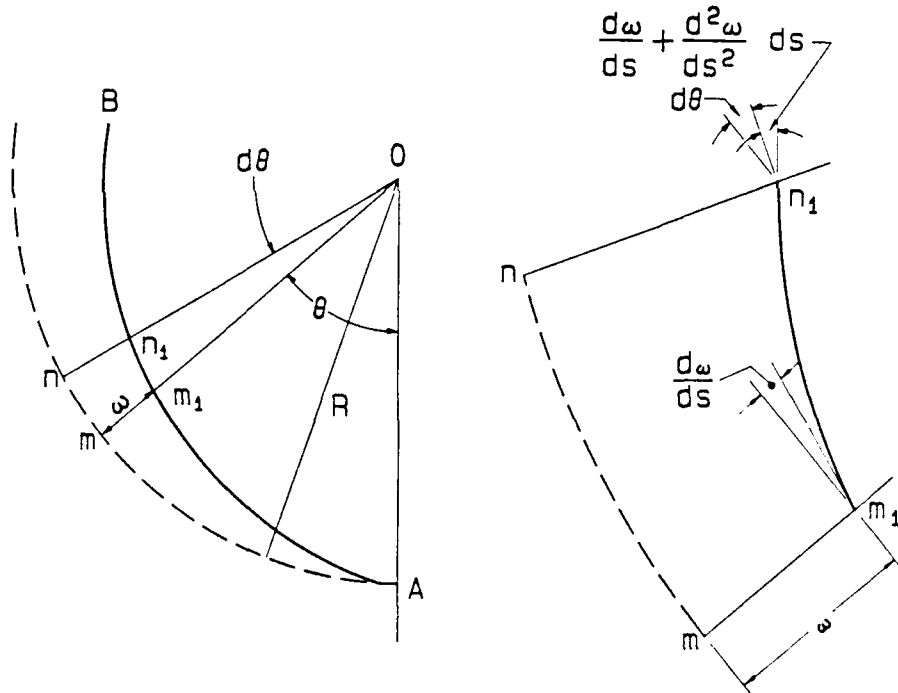

Figure A.1: Geometry of Shell Curvature (from reference [40])

69

The change in length, $\Delta d\phi$, is:

$$ad\phi - (a - w) = -wd\phi = -w\frac{ds}{a}$$

giving the curvature as:

$$\frac{1}{\rho} = \frac{d\phi + (\frac{\partial^2 w}{\partial s^2})ds}{ds(1 - \frac{w}{a})}$$

Neglecting higher order terms, this reduces to:

$$\frac{1}{\rho} = \frac{1}{a}(1 + \frac{w}{a}) + \frac{\partial^2 w}{\partial s^2} = \frac{1}{a}(1 + \frac{w}{a}) + \frac{1}{a^2}\frac{\partial^2 w}{\partial \phi^2}$$

which when substituted into the expression for κ, gives:

$$\kappa = \frac{1}{a^2}(\frac{\partial^2 w}{\partial \phi^2} + w).$$

APPENDIX B: Derivation of the Mathieu Stability Equation

The Mathieu differential equation for parametric instability can be most easily derived for the case of lateral motion of an axially loaded bar [3]. The differential equation for the lateral dynamic motion of a bar under axial loading is:

$$EI\frac{\partial^4 w}{\partial x^4} + P\frac{\partial^2 w}{\partial x^2} + m\frac{\partial^2 w}{\partial t^2} = 0$$

If the axial loading is of a periodic nature, $P(t) = P_o + P_t \cos \phi t$, the equation of motion becomes:

$$EI\frac{\partial^4 w}{\partial x^4} + (P_o + P_t \cos \phi t)\frac{\partial^2 w}{\partial x^2} + m\frac{\partial^2 w}{\partial t^2} = 0$$

If the response is assumed to be periodic, $w(x,t) = f_n(t)\sin\frac{n\pi x}{l}$, the equation becomes:

$$[m\frac{\partial^2 f_n}{\partial t^2} + EI\frac{n^4\pi^4}{l^4}f_n - (P_o + P_t \cos \phi t)\frac{n^2\pi^2}{l^2}f_n]\sin\frac{n\pi x}{l} = 0$$

The internal expression must equal 0, giving:

$$\frac{\partial^2 f}{\partial t^2} + \omega_n^2(1 - \frac{P_o + P_t \cos \phi t}{P_n^*})f_n = 0 \ , \ n = 1,2,3$$

where $\omega_n = \frac{n^2\pi^2}{l^2}\sqrt{\frac{EI}{m}}$ is the free vibration frequency of an unloaded bar and, $P_n^* = \frac{n^2\pi^2}{l^2}EI$, is the Euler buckling load for the bar. This can be rewritten as:

$$f_n'' + \Omega_n^2(1 - 2\mu_n \cos \phi t)f_n = 0$$

which is the traditional form of the Mathieu equation where $\Omega_n = \omega_n\sqrt{\frac{1-P_o}{P_n^*}}$, the bar frequency with applied axial load and $\mu_n = \frac{P_t}{2(P_n^*-P_o)}$, the excitation parameter. The coefficient of f_n approaches zero for certain values of the loading function resulting in instability. The more general case of this function for any periodic loading, $P(t) = P_o + P_t\Phi(t)$, where $\Phi(t+T) = \Phi(t)$, is known as the Hill equation:

$$f'' + \Omega^2[1 - 2\mu\Phi(t)]f = 0$$

Functions f(t), must be found to satisfy this equation. This is difficult except for a few simple cases (see Bolotin[3] and McLachlin[14] for solutions). Parametric resonance of the bar will occur if the excitation frequency is twice the bar frequency, $\phi = 2\Omega$. Regions of instability can be plotted as functions of the parameters, Ω and μ. The shaded regions of Figure B.1 are

regions of instability. The effect of damping on the system is to shift the regions of instability away from the Ω axis as shown in Figure B.2.
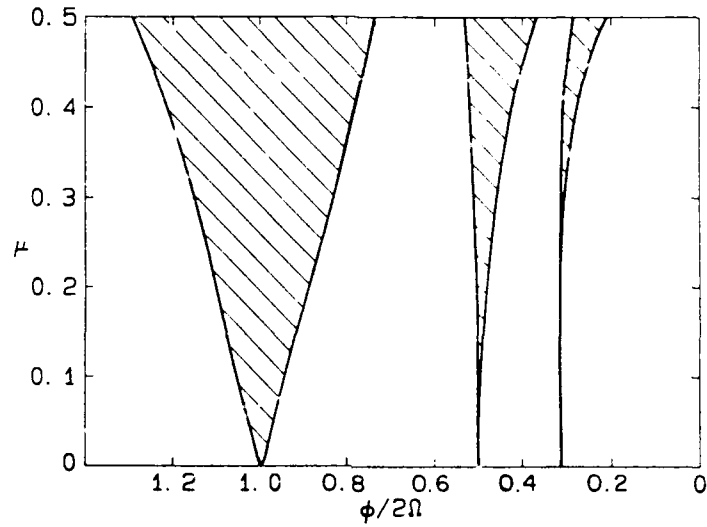

Figure B.1: Regions of Instability from Mathieu Equation (from reference [3])
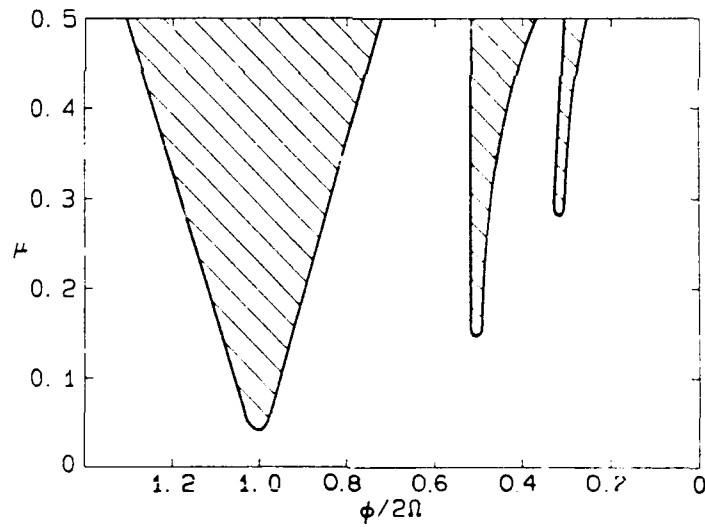

Figure B.2. Regions of Instability with Damping (from reference [3])

References

[1] Hubka W.F., 'Dynamic Buckling of the Elastic Cylindrical Shell Subjected to Impulsive Loading', ASME Transactions, pp 401-406, June 1974.

[2] Lee L.H.N., Horng J.T., 'Inelastic Response of Ring-Stiffened Cylindrical Shells to External Pressure Shock Waves', AIAA Journal, Vol 14, No. 3, March 1976.

[3] Bolotin V.V., 'Dynamic Stability of Elastic Systems', Holden-Day Inc., London, 1964.

[4] Lindberg H.E., Florence A.L., 'Dynamic Pulse Buckling, Theory and Experiment', DNA 6503H, Defence Nuclear Agency Press, Washington, DC, 1983, unlimited distribution.

[5] Lindberg H.E., 'Dynamic Pulse Buckling of Cylindrical Shells', Poulter Laboratory Technical Report 001-70, Stanford Research Institute, Menlo Park, California, April, 1970.

[6] Goodier J.N., 'Dynamic Plastic Buckling', Dynamic Stability of Structures, ed., Herrmann G., Pergamon Press Inc., pp 189-211, New York, 1967.

[7] Jones N., 'Dynamic Elastic and Inelastic Buckling of Shells', in Developments in Thin Walled Structures-2, Elsevier Applied Science Publishers, Essex, England, 1984, pp 49-91.

[8] Lee L.H.N., 'Quasi-Bifurcation in Dynamics of Elastic-Plastic Continua', Journal of Applied Mechanics, No 44, Sept 1977.

[9] Abrahamson G.R., Goodier J.N., 'Dynamic Plastic Flow Buckling of a Cylindrical Shell from Uniform Radial Impulse', Proc. Fourth US National Congress of Appied Mechanics 2, pp 939-950, 1962.

[10] Goodier J.N., McIvor I.K., 'The Elastic Cylindrical Shell Under Nearly Uniform Radial Impulse', Journal of Applied Mechanics, June 1964.

[11] Stuiver W., 'On the Buckling of Rings Subject to Impulsive Pressures', Transactions of the ASME, Journal of Applied Mechanics, Sept 1965.

[12] Abrahamson G.R., 'Critical Velocity for Collapse of a Shell of Circular Cross Section Without Buckling', Journal of Applied Mechanics, pp 407-411, June 1974.

[13] Lindberg H.F., 'Buckling of a Very Thin Cylindrical Shell Due to an Impulsive Pressure' Journal of Applied Mechanics, June 1964.

[14] McLachlin N.W., 'Theory and Application of Mathieu Functions', Dover, New York, 1964.

[15] Yao J.C., 'Dynamic Stability of Cylindrical Shells under Static and Periodic Axial and Radial Loads', AIAA Journal, Vol 1, No 6, June 1963.

[16] Bieniek M.P., Fan T.C., Lackman L.M., 'Dynamic Stability of Cylindrical Shells', AIAA Journal, No 3, March, 1966.

[17] Kalnins A., 'Dynamic Buckling of Axisymmetric Shells', Journal of Applied Mechanics, pp 1063-1068, December 1974.

[18] Wesenberg D.L., 'Elastic-Plastic Buckling of Aluminum Cylindrical Shells Subjected to Axisymmetric Impulse Loads', Journal of Applied Mechanics, pp 985-988, December 1974.

[19] Anderson D.L., Lindberg H.E., 'Dynamic Pulse Buckling of Cylindrical Shells under Transient Lateral Pressures', AIAA Journal, Vol 6, No 4, pp 589-598, April 1968.

[20] Florence A., Vaughan H., 'Dynamic Plastic Flow Buckling of Short Cylindrical Shells Due to Impulsive Loading', J. Solids and Structures, Vol 4, 1968.

[21] Vaughan H., Florence A.L., 'Plastic Flow Buckling of Cylindrical Shells Due to Impulsive Loading', Transactions of the ASME, Journal of Applied Mechanics, March 1970.

[22] Hill R., 'The Mathematical Theory of Plasticity', Oxford Press, Toronto, 1950.

[23] McIvor I.K., Lovell E.G., 'Dynamic Response of Finite-Length Cylindrical Shells to Nearly Uniform Radical Impulse', AIAA Journal, Vol 4, 1968.

[24] Yamaki N.,Elastic Stability of Circular Cylindrical Shells, Elsevier Science Publishers B.V., The Netherlands, 1984.

[25] Nachbar W., 'The Effect of Finite Pressure-Pulse Duration on the Uniform Deformation of a Long Cylindrical Shell', Transactions of the ASME, Journal of Applied Mechanics, June 1965.

[26] Lindberg H.E., Kennedy T.C., 'Dynamic Plastic Pulse Buckling Beyond Strain-Rate Reversal', Journal of Applied Mechanics, June 1975.

[27] Almroth B.O., 'Buckling of a Cylindrical Shell Subjected to Nonuniform External Pressure', Journal of Applied Mechanics, Dec 1962.

[28] S.R. Bodner, P.S. Symonds,'Experimental and Theoretical Investigations of the Plastic Deformation of Cantilever Beams Subjected to Impulse Loading', J. Applied Mechanics, 29, 1962.

[29] Ishizaki T., Bathe KJ., 'On Finite Element Large Displacement and Elastic-Plastic Dynamic Analysis of Shell Structures', Computers and Structures, Vol 12, pp 309-318, Pergamon Press Ltd., 1980.

[30] 'ADINA, A Finite Element Program for Automatic Dynamic Incremental Nonlinear Analysis', User's Manual, ADINA Engineering Inc., Watertown, Mass, Sept. 1981.

[31] Bathe K-J.,Finite Element Procedures in Engineering Analysis, Prentice-Hall Inc, 1982.

[32] Klein S.,'The Nonlinear Dynamic Analysis of Shells of Revolution With Asymmetric Properties by the Finite Element Method', Journal of Pressure Vessel Technology, August, 1975.

[33] Gefken P.R., Kirkpatrick S.W., Holmes B.S., 'Reponse of Impulsively Loaded Cylindrical Shells', International Journal of Impact Engineering, Vol 7, No 2, 1988.

[34] Kirkpatrick S.W., Holmes B.S., 'Structural Response of Thin Cylindrical Shells Subjected to Impulsive External Loads', AIAA Journal, Vol 26, No 1, 1987.

[35] Kirkpatrick S.W., Holmes B.S.,'The Effect of Initial Imperfections on Dynamic Buckling of Shells', ASCE Journal of Engineering Mechanics, Vol 115, No 5, 1989.

[36] Wu R.W.H., Witmer E.A., 'Theoretical and Experimental Studies of Transient Elastic-Plastic Large Deflections of Geometrically Stiffened Rings', Journal of Applied Mechanics, No 42, Dec 1975.

[37] Lee L.H., Horr J.T., 'Inelastic Response of Ring-Stiffened Cylindrical Shells to External Pressure Pulses',Office of Naval Research Technical Report Number UND-75-1, March, 1975, distribution unlimited.

[38] Haxton R.S., Haywood J.H., 'Linear Elastic Response of a Ring Stiffened Cylinder to Underwater Explosion Loading', Advances in Marine Structures, ARE, Dunfermline, Scotland, May 1986.

[39] Everstine G.C.,'A NASTRAN Implementation of the Doubly Asymptotic Approximation for Underwater Shock Response', Proceedings of the 5th NASTRAN User's Colloquium, October, 1976.

[40] Timoshenko S.P., Cere J.M.,Theory of Elastic Stability, McGra·   ∪o., Toronto, 1961.

DOCUMENT CONTROL DATA

(Security classification of title, body of abstract and indexing annotation must be entered when the overall document is classified)

1. ORIGINATOR (the name and address of the organization preparing the document. Organizations for whom the document was prepared, e.g. Establishment sponsoring a contractor's report, or tasking agency, are entered in section 8.) Defence Research Establishment Atlantic	2. SECURITY CLASSIFICATION (overall security classification of the document, including special warning terms if applicable) UNCLASSIFIED

3. TITLE (the complete document title as indicated on the title page. Its classification should be indicated by the appropriate abbreviation (S,C,R or U) in parentheses after the title.)

A Review of the Theory and Methods for Determining Dynamic Pulse buckling of Cylindical Shells

4. AUTHORS (Last name, first name, middle initial. If military, show rank, e.g. Doe, Maj. John E.)

Pegg, Neil G.

5. DATE OF PUBLICATION (month and year of publication of document) September 1989	6a. NO. OF PAGES (total containing information. Include Annexes, Appendices, etc.) 86	6b. NO. OF REFS (total cited in document) 40

6. DESCRIPTIVE NOTES (the category of the document, e.g. technical report, technical note or memorandum. If appropriate, enter the type of report, e.g. interim, progress, summary, annual or final. Give the inclusive dates when a specific reporting period is covered.)

Technical Memorandum

8. SPONSORING ACTIVITY (the name of the department project office or laboratory sponsoring the research and development. Include the address.)

9a. PROJECT OR GRANT NO. (if appropriate, the applicable research and development project or grant number under which the document was written. Please specify whether project or grant) 1AH	9b. CONTRACT NO. (if appropriate, the applicable number under which the document was written)

10a. ORIGINATOR'S DOCUMENT NUMBER (the official document number by which the document is identified by the originating activity. This number must be unique to this document.) DREA Technical Memorandum 89/222	10b. OTHER DOCUMENT NOS. (any other numbers which may be assigned this document either by the originator or by the sponsor)

11. DOCUMENT AVAILABILITY (any limitations on further dissemination of the document, other than those imposed by security classification)

(X) Unlimited distribution
( ) Distribution limited to defence departments and defence contractors; further distribution only as approved
( ) Distribution limited to defence departments and Canadian defence contractors; further distribution only as approved
( ) Distribution limited to government departments and agencies; further distribution only as approved
( ) Distribution limited to defence departments; further distribution only as approved
( ) Other (please specify):

12. DOCUMENT ANNOUNCEMENT (any limitations to the bibliographic announcement of this document. This will normally correspond to the Document Availability (11). However, where futher distribution (beyond the audience specified in 11) is possible, a wider announcement audience may be selected.)

13. ABSTRACT (a brief and factual summary of the document. It may also appear elsewhere in the body of the document itself. It is highly desirable that the abstract of classified documents be unclassified. Each paragraph of the abstract shall begin with an indication of the security classification of the information in the paragraph (unless the document itself is unclassified) represented as (S), (C), (R), or (U). It is not necessary to include here abstracts in both official languages unless the text is bilingual).

A review of theoretical developments in predicting the buckling response of cylinders subject to impulsive loads is presented. Most of this theory has dealt with axisymmetric, radial impulses on cylinders. The development of solutions for the critical modes and loading magnitudes which produce unbounded growth of displacements are reviewed. Existing theories cover the specific cases of either entirely elastic or entirely plastic material behaviour for infinite length and short cylindrical shells. The resultant theories are applied to various shell geometries to investigate influencial parameters. A review of numerical finite element and finite difference studies investigating dynamic pulse buckling is also given. The requirements to investigate dynamic buckling of more complex structures such as ring stiffened cylinders are discussed.

14. KEYWORDS, DESCRIPTORS or IDENTIFIERS (technically meaningful terms or short phrases that characterize a document and could be helpful in cataloguing the document. They should be selected so that no security classification is required. Identifiers, such as equipment model designation, trade name, military project code name, geographic location may also be included. If possible keywords should be selected from a published thesaurus. e.g. Thesaurus of Engineering and Scientific Terms (TEST) and that thesaurus-identified. If it is not possible to select indexing terms which are Unclassified, the classification of each should be indicated as with the title.)

Cylinders
Dynamics
Buckling
Submarines
Pulse buckling
Stability